



# Master Thesis

## **Multi-stage MPC of Agricultural Biogas Plants with Uncertain Substrate Characterization**

Fakultät III Prozesswissenschaften  
Institut Prozess- und Verfahrenstechnik  
Chair of Control

**B. Sc. Julius Ferdinand Frontzek**  
(Matriculation Number: 455301)

Supervisors:  
M. Sc. Terrance Wilms  
Prof. Dr. Steffi Knorn  
M. Sc. Simon Hellmann (DBFZ)

February 26, 2024







# **Eigenständigkeitserklärung**

Hiermit erkläre ich, dass ich die vorliegende Arbeit selbstständig und eigenhändig sowie ohne unerlaubte fremde Hilfe und ausschließlich unter Verwendung der aufgeführten Quellen und Hilfsmittel angefertigt habe.

Berlin, den 26.02.2024

.....

Unterschrift



# **Foreword**

This thesis was conducted during my time at the Deutsches Biomassforschungszentrum gemeinnützige GmbH (DBFZ), which I would like to thank for this opportunity.

I would like to express my profound appreciation to my supervisor, Simon Hellmann, for his exceptional guidance and support throughout this project. Additionally, his efforts enabled me to attend the 6th Doctoral Colloquium BIOENERGY, which partly contributed to my decision to continue in research after completing this thesis. I am equally grateful to my other supervisor, Terrance Wilms, for providing me the opportunity to undertake this thesis and for his continual supply of inspiring ideas and constructive feedback during this period.

Additionally, I extend my gratitude to Prof. Dr. Steffi Knorn for her valuable insights and constructive feedback during the course of this thesis. I am equally thankful for her role in sparking my interest in the field of controls through her numerous lectures. I would also like to thank my parents for both their financial and emotional support throughout my life to date. Last but certainly not least, I would like to thank my friends and other family members for accompanying me in my life!

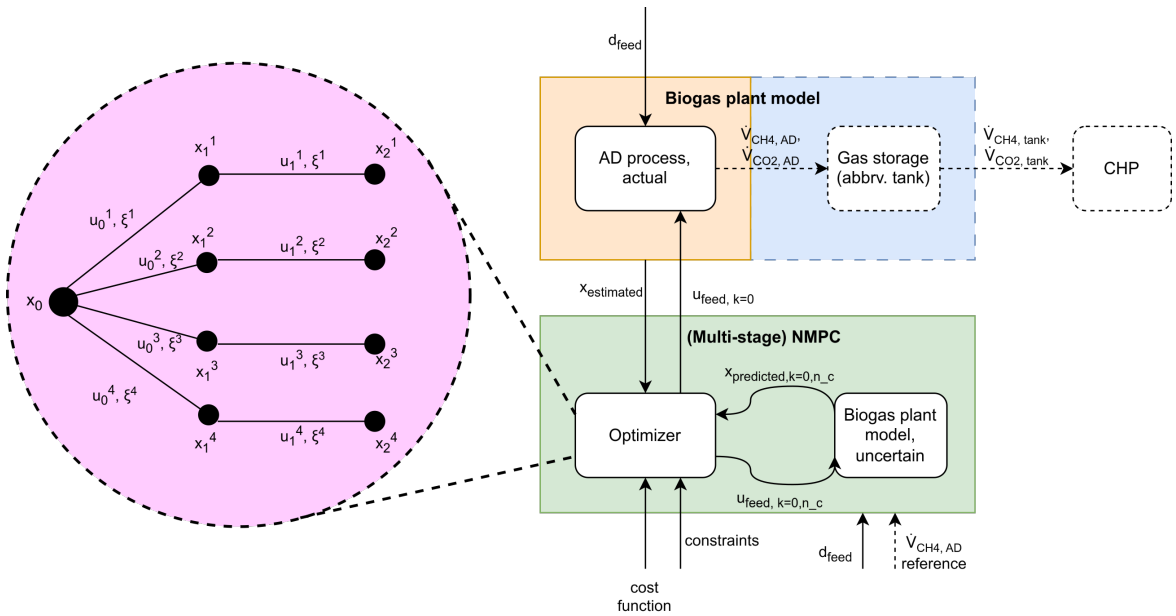


# Contents

List of Figures . . . . .	XIII
List of Tables . . . . .	XV
Nomenclature . . . . .	XVIII
<b>1 Introduction</b>	<b>1</b>
<b>2 Methods</b>	<b>5</b>
2.1 Dynamic Model . . . . .	5
2.1.1 Normalization . . . . .	6
2.2 Linear Uncertainty Propagation . . . . .	6
2.3 Orthogonal Collocation on Finite Elements . . . . .	6
2.4 Multi-Stage Nonlinear Model Predictive Control . . . . .	7
<b>3 Implementation</b>	<b>9</b>
3.1 Substrate Composition Uncertainties . . . . .	9
3.1.1 Uncertainty Sources . . . . .	9
3.1.2 Uncertainty Propagation . . . . .	10
3.2 Disturbance Feeding . . . . .	13
3.3 Multi-stage Scenarios . . . . .	13
3.4 Gas Storage Model . . . . .	14
3.5 Application Scenarios . . . . .	17
3.5.1 Scenario 1 . . . . .	17
3.5.2 Scenario 2 . . . . .	18
3.6 Biogas Plant Dimensioning . . . . .	19
3.7 Simulation Initialization . . . . .	20
3.8 Cost Functions And Constraints . . . . .	20
3.9 Software . . . . .	23
<b>4 Results and Discussion</b>	<b>25</b>
4.1 Methanation . . . . .	25
4.2 Cogeneration . . . . .	29
4.3 Runtime Analysis . . . . .	37

4.4 Controller Stability . . . . .	38
4.5 Limitations and Assumptions . . . . .	39
<b>5 Theses</b>	<b>41</b>
<b>6 Extended Conclusions and Outlook</b>	<b>43</b>
<b>Appendix</b>	<b>49</b>
A.1 Normalized Equations of ADM1-R3-frac . . . . .	49
A.2 State Vector . . . . .	52
A.3 Parameters . . . . .	53
A.3.1 Substrates . . . . .	53
A.3.2 Normalization Vectors . . . . .	54
A.3.3 Substrate Costs . . . . .	55
A.4 Software - UML Diagrams . . . . .	55
A.5 DOC 2023 . . . . .	60

# Graphical Abstract





# Abstract

In spite of the ongoing energy transition towards renewable energy sources, the prospects for biogas generation through agricultural anaerobic digestion (AD) plants are often overlooked. And yet it poses a controllable renewable energy source, capable of generating electricity at times of high demand independent of current weather conditions. This very property motivates the development of a substrate feed control capable of offsetting an AD plant's usually high levelized costs of electricity (LCOE) by generating well renumerated electricity at times of unfulfilled demand. To achieve this goal, a multi-stage nonlinear model predictive control (NMPC) was designed with the Python library `do-mpc` to compute optimal substrate feedings into the AD plant. In conducted simulation studies the NMPC proved to be capable of tracking methane volume flow demands of a flexibly operated combined heat and power plant (CHP) plant. The chosen robust multi-stage NMPC approach was able to satisfy filling level constraints posed by the developed gas storage model while dealing with uncertain compositions of substrate macronutrients. Additionally, a nominal NMPC was developed which successfully tracked setpoints of predefined methane volume flow setpoints. Both controllers rejected disturbances posed by random feeding errors and disturbance feeding flows to satisfaction. Upon the implementation of soft sensors, experimental studies followed by real-life applications are deemed feasible. Thereby, the present thesis contributed to the further development of flexible AD plant operation in the future.



# Zusammenfassung

Trotz der laufenden Energiewende wird das Potential für die Biogaserzeugung durch anaerobe Vergärung in landwirtschaftlichen Biogasanlagen oft übersehen. Gleichwohl handelt es sich um eine steuerbare regenerative Energiequelle, die auf Abruf unabhängig von den aktuellen Wetterbedingungen Strom erzeugen kann. Genau diese Eigenschaft motiviert die Entwicklung einer Regelung der Substratzufuhr, die in der Lage ist, die typischerweise hohen Stromgestehungskosten einer Biogasanlage durch die Erzeugung von Strom zu Tageszeiten mit hohen Börsenstrompreisen auszugleichen. Um dieses Ziel zu erreichen, wurde eine nichlineare modellprädiktive Regelung (NMPC) mit der Python-Bibliothek `do-mpc` entwickelt, um die optimalen Substratfütterungsmengen in die Biogasanlage zu berechnen. In durchgeführten Simulationsstudien wurde demonstriert, dass die geregelte Anlage dem Methan-Volumenstrombedarf eines flexibel betriebenen Blockheizkraftwerks folgen kann. Der gewählte robuste "multi-stage NMPC" Ansatz war in der Lage, die durch das entwickelte Gasspeichermodell vorgegebenen Füllstandsrandbedingungen zu erfüllen und gleichzeitig mit unsicheren Zusammensetzungen der Substratmakronährstoffe umzugehen. Zusätzlich wurde eine nominale modellprädiktive Regelung entwickelt, die erfolgreich vordefinierten Methan-Volumenstrom-Sollwerten folgte. Beide Regler konnten die Einflüsse von Störungen unterdrücken, die durch zufällige Einspeisefehler und Störsubstratfütterungen verursacht wurden. Sobald Soft-Sensoren implementiert sind, werden experimentelle Studien und anschließende reale Anwendungen für realisierbar erachtet. Somit trug diese Arbeit zu künftigen Weiterentwicklungen im Bereich flexibler Biogaserzeugung bei.



# List of Figures

2.1	Schematic illustration of OCFE . . . . .	7
2.2	Schematic illustration of scenario tree used in Multi-stage NMPC . . . . .	8
3.3	Probability density functions for fermentable fractions of macronutrients	12
3.4	Multi-stage scenario tree with robust horizon $N_r = 1$ . . . . .	14
3.5	Cost function shape for Scenario 2 with respect to filling level . . . . .	23
4.6	Scenario 1a results with linear substrate cost formulation . . . . .	26
4.7	Scenario 1a results with quadratic substrate cost formulation . . . . .	27
4.8	Scenario 1b results . . . . .	29
4.9	Scenario 2a results . . . . .	32
4.10	Scenario 2b results . . . . .	34
4.11	Scenario 2c results . . . . .	36
4.12	Boxplot of NMPC iteration runtimes . . . . .	38
A.13	UML class diagram for simulation code . . . . .	56
A.14	UML class diagram for plotting code . . . . .	57
A.15	UML package diagram . . . . .	58
A.16	Poster presented at the 6th Doctoral Colloquium BIOENERGY . . . . .	60



# List of Tables

3.1	Nominal values required for uncertainty propagation computations . . . . .	11
3.2	Variation coefficients required for uncertainty propagation computations	12
3.3	CHP operating schedule . . . . .	18
3.4	Dimensions of the simulated digester, gas storage and CHP plant . . . . .	19
3.5	Cost function coefficients Scenario 1 . . . . .	21
3.6	Cost function coefficients Scenario 2 . . . . .	23
4.1	Horizon lengths applied to Scenario 1 . . . . .	25
4.2	Horizon lengths applied to Scenario 2 . . . . .	30
A.1	Description of state vector components . . . . .	52
A.2	Values of inlet concentrations . . . . .	53
A.3	State normalization vector $\underline{T}_x$ . . . . .	54
A.4	Input normalization vector $\underline{T}_u$ . . . . .	54
A.5	Costs of individual substrates . . . . .	55

## Nomenclature

Variable	Unit	Meaning
<b>General Notation</b>		
$a$		scalar quantity
$\bar{a}$		normalized quantity
$\bar{a}$		dry matter based quantity
$\underline{a}$		vector quantity
<b>A</b>		matrix
<b>Latin Letters</b>		
<b>F</b>	—	system matrix
<b>H</b>	—	measurement matrix
$p$	bar	pressure
$t$	s	time
$u$	—	input
$x$	—	state
$V$	$m^3$	Volume
<b>Greek Letters</b>		
$\Delta$	—	difference
$\rho$	$kg/m^3$	density
$\Sigma$	—	sum
$\sigma$	—	standard deviation

---

Abbreviations	Meaning
AD	Anaerobic Digestion
ash	Ash
BMP	Biochemical Methane Potential
ch	Carbohydrates
CHP	Combined Heat and Power
CM	Cattle Manure
COD	Chemical Oxygen Demand
CS	Corn Silage
DM	Dry Matter
EKF	Extended Kalman Filter
FM	Fresh Matter
FoDM	Fermentable organic Dry Matter
GS	Grass Silage
HAWK	Hochschule für angewandte Wissenschaft und Kunst Hildesheim/Holzminden/Göttingen
IPOPT	Interior Point Optimizer
LCOE	Levelized Cost of Electricity
li	Lipids
MIMO	Multiple Input Multiple Output
MLU	Manure with Larger Uncertainty
MPC	Model Predictive Control
$N_c$	Control Horizon
NMPC	Nonlinear Model Predictive Control
$N_p$	Prediction Horizon
$N_r$	Robust Horizon
OCFE	Orthogonal Collocation on Finite Elements
pr	Proteins
SBS	Sugar Beet Silage
UKF	Unscented Kalman Filter
VC	Variation Coefficient

# 1 Introduction

Upon reaching the end of their 20 year EEG funding period, many of Germany's over 9000 biogas plants are facing reduced revenues generated from their electrical power production as described by Gusewell et al. [16]. This may lead to the closing of a substantial amount of these biogas plants. In the face of Germany's ambitious efforts to switch to renewable energy sources, the demise of this technology could not only send discouraging political signals but these plants may actually play an important part in ensuring energy safety. As opposed to wind and solar energy, power generated from biogas through anaerobic digestion (AD) does not rely on fluctuating and uncontrollable weather phenomena. Instead, the process itself is controllable and additionally allows for the buffering of the generated biogas before combusting it for electricity and heat generation [11].

However, continued operation of German AD plants in the given competitive renewable electricity market requires to employ strategies to increase their generated revenues, decrease their costs or both. One of the main evolving strategies is the flexibilization of an biogas plant, meaning the generation of electricity at peak load times in the country or continent at both higher market prices as well as with flexibilization premiums [29]. To facilitate a more flexible generation of electricity from biogas plants, it is crucial that a sufficiently large volume of biogas is available for combustion in a combined heat and power (CHP) plant at times of high demand. At the same time, it needs to be ensured that the installed gas storage does not exceed its capacity while the CHP plant is turned off. One way to achieve this would be the installation of additional gas storage tanks in existing agricultural biogas plants while continuing to generate biogas quasi-stationary in the AD process. Another approach is the flexible generation of biogas according to predicted demand. This can be achieved by controlling the amount and composition of substrates fed into the AD plant. This has the potential to flexibilize the process while keeping the already installed gas storage capacity and is considered in one of the two main application scenarios of this thesis. The other main strategy described by [29], the upgrading of biomethane through methanation was also accounted for in this thesis in the other main application scenario.

Another envisioned strategy for better profitability of AD plants is the reduction of gross substrate costs for the operator. While there may exist other approaches to

achieve this, two of them shall be outlined here. The first one is the usage of organic waste as substrates that are provided at little to no cost to the operator or even for a profit. The second one is the renunciation of substrate composition measurements either for regular substrates or for the described organic waste substrates. Instead, educated guesses about the substrate composition could be drawn from look-up tables for similar, previously measured substrates and thus eliminating laboratory costs. As the estimation of substrate composition introduces larger uncertainties, it may require a robust control approach to assure non-violation of constraints such as upper and lower gas storage limits.

While the control of AD has been extensively studied in the treatment of wastewater [3], [26], [25], Gaida et al. [14] showed that there exists far less research in the context of agricultural AD plants. Some existing research in substrate control for agricultural AD plants includes the development of a Nonlinear Model Predictive Control (NMPC) by Xue et al. [20]. However, their control focused on optimal steady-state plant operation on long time scales rather than flexible biogas generation. Further, Mauky et al. [24] as well as Raeyatdoost et al. [28] developed controllers for biogas generation used in flexibly operated CHP plants with NMPC or PI controllers, respectively. The controller developed by Mauky et al. was shown to control AD plants with a significantly larger ratio of CHP power to gas storage size as compared to the one developed by Raeyatdoost et al. It was also successfully demonstrated on two differently sized real-life plants.

Models used in control systems of previous AD research were typically relatively simple both in water treatment as well as in agricultural AD plants. Many of them do not allow to monitor process stability indicators such as the pH value of the digester or assumed a separate control system for a stabilized acidity of the biogas plant [32]. Therefore, in this thesis we applied the more elaborate model ADM1-R3, which was proposed by Weinrich and Nelles [35] and considers three different inhibition processes. Weinrich and Nelles simplified the well-known ADM1 [6] and transformed the original formulation based on Chemical Oxygen Demand (COD) to a mass based one. This allowed practical application in control schemes and in an agricultural context. Their model simplifications were achieved by summarizing degradation pathways, thus reducing the number of required states and parameters. The simplified ADM1-R3 has been validated by Weinrich et al. in three different experimental setups [34].

In this thesis it was sought to design a robust control system for a modified version of the ADM1-R3 capable of controlling the AD process with multiple input feeds. Key aspects that motivated to choose an NMPC scheme for this task were the nonlinearities of the ADM1-R3, its multiple input multiple output (MIMO) structure as well as potential system constraints. The suitability of NMPC schemes for such con-

trol tasks has been described by [10]. As for robust extensions of model predictive control (MPC) or the more general NMPC, there exist several approaches. Some of most popular ones as described by [26] include tube-based MPC, min-max MPC, and multi-stage NMPC. Further, stochastic MPC formulations have also been used in the literature to address model uncertainties [17], [27]. In this thesis a multi-stage NMPC was implemented for constraint critical applications. The application of this method was partly motivated by its less conservative nature as compared to min-max MPC [22] as well as by its accessibility due to the contribution of the free and open-source Python library `do-mpc` by Fiedler et al. [12]. This work examines the suitability of `do-mpc` based control implementations for controlling an AD plant that is fed with substrates of uncertain macronutrient composition.

This research involves two simulation scenarios: One is constant biogas production aimed at biogas upgrading to biomethane (methanation). The other is flexible co-generation, i.e. the generation of electricity and heat in a CHP plant. To this end, two NMPC controllers were designed and tested in five different sub-scenarios and examined for their capability in handling uncertain compositions of the utilized substrates' macronutrients. In case of the cogeneration scenario special focus was put on the satisfaction of constraints posed by the capacity limits of the gas storage.

The remainder of this thesis is structured as follows. In Chapter 2 theoretical concepts used in this work are described. The following Chapter 3 lays out the developed methodology and implementation details. The results of the different application scenarios are presented and discussed in Chapter 4. Afterwards, seven theses based on the findings are formulated in Chapter 5 before the conclusions of this work are drawn in Chapter 6.



# 2 Methods

This chapter briefly describes the AD model used in this thesis as well as some theoretical overviews about uncertainty propagation, orthogonal collocation on finite elements and multi-stage model predictive control, which have all been applied in this thesis.

## 2.1 Dynamic Model

The Anaerobic Digestion Model No. 1 (ADM1) proposed by Batstone et al. [6] is widely recognized as the benchmark for AD process modeling. However, its complex model structure prevents its application in monitoring and control. Instead, a modified version of the mass-based simplification ADM1-R3, formulated by Weinrich and Nelles [35], was used for this research. 'R3' denotes the proposed third simplification stage. As opposed to preceding simplifications, this model combines the formation of different organic acids to a single acid concentration,  $S_{ac}$ . This state plays a key role in the modeling of pH-based microbial growth inhibition. Two other inhibition phenomena are also modeled, namely inhibition through high ammonia concentrations and nitrogen depletion.

The model differentiates between a liquid and a gaseous phase. Concentrations of soluble or gaseous (S) and particulate (X) components within these phases comprise a total of 17 states in the ADM1-R3. Some key states shall be noted which include the concentrations of the macronutrients carbohydrates, proteins and lipids in the liquid phase,  $X_{ch}$ ,  $X_{pr}$  and  $X_{li}$ . Microbial biomass concentrations are reflected by the states  $X_{bac}$  and  $X_{ac}$ .  $X_{ash}$  represents the ash concentration in the liquid phase. Further, concentrations of methane ( $CH_4$ ) and carbon dioxide ( $CO_2$ ) in the gaseous phase of the AD plant are described by  $S_{ch4,gas}$  and  $S_{co2,gas}$ . A combination of these two states comprises the output variable  $\dot{V}_g$  representing the total volume outflow of biogas from the AD plant. This output variable has later been used together with the output variables  $p_{CH_4}$  and  $p_{CO_2}$  to model the external gas storage. Another output variable,  $pH$ , has been observed for process stability analyses.

A modification to this model encompassed the division of the carbohydrate state into a fraction of long-chained, slowly digestible carbohydrates  $X_{ch,s}$  as well as short-chained, fast digestible carbohydrates  $X_{ch,f}$ , leading to the model name ADM1-R3-frac with a

total of 18 states:

$$\underline{x} = \left[ S_{\text{ac}}, S_{\text{ch4}}, S_{\text{IC}}, S_{\text{IN}}, S_{\text{h2o}}, X_{\text{ch,f}}, X_{\text{ch,s}}, X_{\text{pr}}, X_{\text{li}}, X_{\text{bac}}, X_{\text{ac}}, X_{\text{ash}}, \dots S_{\text{ion}}, S_{\text{ac}^-}, S_{\text{hco}_3^-}, S_{\text{nh3}}, S_{\text{ch4,gas}}, S_{\text{co2,gas}} \right]^T \quad (2.1)$$

A brief description of all states is provided in Table A.1 in the appendix.

### 2.1.1 Normalization

A normalization for states and inputs was carried out to improve numerical stability of the NMPC optimization problem. All 18 AD states were normalized to their respective maximum absolute value observed during the preceding steady state simulation. The substrate feed inputs were normalized to the maximum feeding values for the respective conveyor augers or pumps which differed for manures and silages. These were based on physical limitations of the biogas plant at DBFZ and are reported along with other dimensioning parameters in Table 3.4.

The normalization vectors and the normalized ADM1-R3-frc are reported in Appendices A.3.2 and A.1, respectively.

## 2.2 Linear Uncertainty Propagation

Given a variable  $y$  which is a function of variables  $x_1, \dots, x_n$ , i.e.  $y = y(x_1, \dots, x_n)$ , its statistical moments are also a function of the moments of  $x_1, \dots, x_n$ . The propagation of its moments under the assumption of independence of the variables is described by [19]. Reformulation of the variance propagation leads to the following propagation scheme for standard deviations  $\sigma$ :

$$\sigma_y = \sqrt{\sum_{i=1}^n \left( \frac{\partial y}{\partial x_i} \cdot \sigma_{x_i} \right)^2}. \quad (2.2)$$

## 2.3 Orthogonal Collocation on Finite Elements

Since the application of `do-mpc` requires a fully discretized system, the time continuous ordinary differential equations of the ADM1-R3-frc were discretized via orthogonal collocation on finite elements (OCFE) [13]. This approach involves the discretization of time into so called finite elements. Within a finite element, the solution of the respective differential equation is approximated as the sum of parametrized trial functions. It is then demanded that this approximation must be exact at a set of previously defined collocation points that lie within the finite element. This leads to

a set of algebraic equations which must be solved for the unknown parameters of the trial functions. The sum of these trial functions with now known parameters yields the solution to the problem. Figure 2.1 displays an illustration of the OCFE scheme as reported in [7].

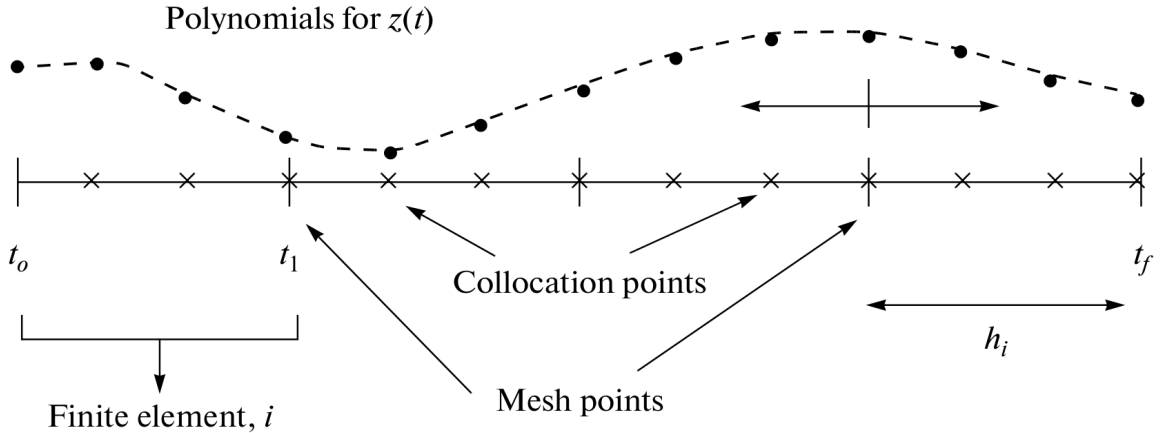


Figure 2.1: Schematic illustration of OCFE as shown in [7]

## 2.4 Multi-Stage Nonlinear Model Predictive Control

Multi-stage Nonlinear Model Predictive Control is an NMPC scheme which aims to robustify the controller performance with respect to parametric model uncertainties. The concept was first introduced in [8] and subsequently named multi-stage NMPC by Lucia et al. [22]. The method explicitly considers parametric uncertainties. This is also where its main assumption lies, namely that all considered uncertainties have discrete values only. This assumption allows for the construction of a scenario tree as shown in Figure 2.2. It creates a so called scenario tree, the core of this method, where at each time step all parametric uncertainties are combined with each other. Each combination of uncertainty realizations  $d_i^j$  is denoted by the index  $j$  in Figure 2.2.

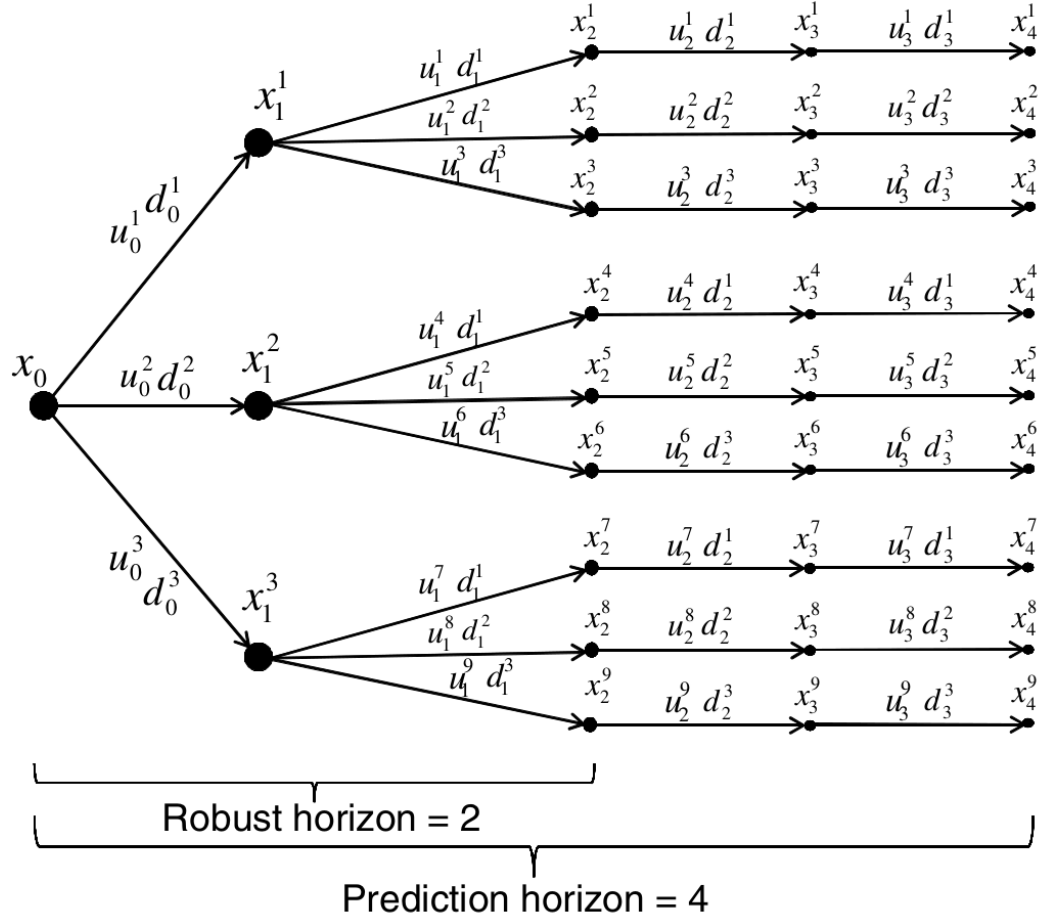


Figure 2.2: Schematic illustration of scenario tree used in multi-stage NMPC as shown in [21]

This creation of branches is then repeated at every time step until a specified robust horizon, after which the uncertainties are assumed to take the values of the last combination. Each of the leaf nodes represents a scenario. This is where the decrease of conservativeness in its control performance comes from as opposed to min-max MPC: while min-max MPC only minimizes its specified cost function for the worst-case scenario, multi-stage NMPC minimizes the weighted summation of the cost function across all scenarios represented in the scenario tree. These weights represent the probability that the respective scenario occurs [22], [21].

Lucia and Engell reported in [21] that constraint satisfaction can only be guaranteed if the parametric uncertainties take the discrete values considered in the scenario tree. However, they also stated that even in nonlinear systems the construction of the scenario tree with the upper and lower limits of uncertain parameters usually leads to constraint satisfaction [21]. This observation will later be applied in the construction of the scenario tree in this thesis.

# 3 Implementation

This chapter discusses implementation details of this thesis. Firstly, the consideration of uncertainties is laid out, followed by the description of disturbance feedings. Afterwards, the consideration of uncertainties encountered in input and disturbance modeling of an external gas storage application scenarios are described. Some further implementation details include the dimensioning of the AD plant, the initialization of simulations as well as explanations on the applied cost functions and software.

## 3.1 Substrate Composition Uncertainties

While the model input of the ADM1-R3-frac solely consists of the volume flow of the respective substrates into the AD plant, their composition is of equal importance. Substrate compositions in the ADM1-R3-frac are described by vectors  $\xi$  which contain the inlet concentrations in the same structure as the components contained in the state vector. There only exist 12 non-zero inlet concentrations since some of these concentrations describe chemical intermediates or end products of the AD process. In real-life applications, all of these concentrations have a certain degree of uncertainty. However, the three macronutrients (carbohydrates, proteins and lipids) assume the largest concentrations and are particularly uncertain. That is because of a large degree of uncertainty in their fermentability, i.e. the degree to which they can be fermented by the microorganisms in the AD process. This motivates the decision taken in this thesis to explicitly take into account the effect of uncertainties posed by the concentrations of macronutrients. Additional uncertainties of parametric or structural nature were not considered.

The substrates used in this thesis were grass silage (GS), corn silage (CS), sugar beet silage (SBS) and cattle manure (CM).

### 3.1.1 Uncertainty Sources

The macronutrient concentrations contained in the inlet concentration vector  $\xi$  describe the fermentable fraction of the respective macronutrient. These are however not measured directly in practice. Instead, only raw macronutrients can be deter-

mined in lab analyses. Further, there exists no deterministic relation between raw and fermentable macronutrients. The unknown error resulting from the approximation of the fermentable fractions is therefore considered as the main model uncertainty.

For known mass density of the fresh matter ( $\rho_{FM}$ ), dry matter ( $DM$ ) fraction, raw macronutrient concentration ( $\bar{X}_i$ ) and fermentation quotient ( $\bar{FQ}_i$ ), the inlet concentrations can be computed as per (3.1). The fermentation quotient denotes the fermentable fraction of the raw macronutrient. Bars denote the reference to DM.

$$\xi_{ch} = \bar{FQ}_{ch} \cdot \bar{X}_{ch} \cdot DM \cdot \rho_{FM} \quad (3.1a)$$

$$\xi_{pr} = \bar{FQ}_{pr} \cdot \bar{X}_{pr} \cdot DM \cdot \rho_{FM} \quad (3.1b)$$

$$\xi_{li} = \bar{FQ}_{li} \cdot \bar{X}_{li} \cdot DM \cdot \rho_{FM}. \quad (3.1c)$$

It was assumed that all proteins and lipids contained in the considered substrates were fully fermentable, i.e.  $\bar{FQ}_{pr} = \bar{FQ}_{li} = 1$ . The latter assumption is sufficiently accurate for agricultural substrates due to their low lipid concentration. The assumption of fully fermentable proteins restricts the scope of this thesis to substrates with low protein concentration. Thus, all non-fermentable macronutrients were attributed to carbohydrates. Under this assumption, the approximated fermentation quotient for carbohydrates  $\bar{FQ}_{ch}$  can then be computed if the total fermentation quotient  $FQ_{total}$  is known:

$$\bar{FQ}_{ch} = \bar{X}_{ch}^{-1} \cdot (FQ_{total} \cdot (1 - \bar{X}_{ash}) - \bar{X}_{pr} - \bar{X}_{li}). \quad (3.2)$$

In this research  $\rho_{FM}$  was considered to be exactly equal to  $1 \text{ g cm}^{-3}$  for each considered substrate.  $\bar{X}_i$  and  $DM$  can be measured relatively quickly [1] or taken from literature [33]. The total fermentation quotients were computed as a substrate's fraction of biochemical methane potential (BMP) per theoretical maximum biochemical methane potential which is reported by Weißbach [36] as  $420 \text{ L/kgFoDM}$  (fermentable organic dry matter). Raw macronutrient concentrations of carbohydrates,  $\bar{X}_{ch}$  were computed as follows:

$$\bar{X}_{ch} = 1 - \bar{X}_{ash} - \bar{X}_{pr} - \bar{X}_{li}. \quad (3.3)$$

Determination of the fermentation quotients  $\bar{FQ}_i$  necessitates time consuming experiments. In a real life scenario  $\bar{FQ}_{ch}$  must be estimated or taken from literature. Moreover, the DM-based values  $\bar{X}_i$  must either be measured or derived from literature data. Since the latter option is cheaper, this procedure was chosen for this thesis.

### 3.1.2 Uncertainty Propagation

It was assumed that uncertainties resulting from different influencing factors were independent of one another. This simplification allows for the application of the uncer-

tainty propagation described in Section 2.2. These propagations were initially derived analytically but later implemented using the Python package `uncertainties`. Applying (2.2) to (3.1) with known mass density of fresh matter, the standard deviation of the inlet concentration of carbohydrates  $\sigma_{\xi_{ch}}$  is propagated as follows:

$$\sigma_{\xi_{ch}} = \sqrt{(\bar{X}_{ch} \cdot DM \cdot \rho_{FM} \cdot \sigma_{\bar{FQ}_{ch}})^2 + (\bar{FQ}_{ch} \cdot DM \cdot \rho_{FM} \cdot \sigma_{\bar{X}_{ch}})^2 + (\bar{FQ}_{ch} \cdot \bar{X}_{ch} \cdot \rho_{FM} \cdot \sigma_{DM})^2}. \quad (3.4)$$

Corresponding equations can be formulated for the proteins and lipids which do not include the term related to the respective fermentation quotient as they were assumed to be equal to one for both proteins and lipids as stated in Section 3.1.1.

$$\sigma_{\xi_{pr}} = \sqrt{(\bar{FQ}_{pr} \cdot DM \cdot \rho_{FM} \cdot \sigma_{\bar{X}_{pr}})^2 + (\bar{FQ}_{pr} \cdot \bar{X}_{pr} \cdot \rho_{FM} \cdot \sigma_{DM})^2} \quad (3.5)$$

$$\sigma_{\xi_{li}} = \sqrt{(\bar{FQ}_{li} \cdot DM \cdot \rho_{FM} \cdot \sigma_{\bar{X}_{li}})^2 + (\bar{FQ}_{li} \cdot \bar{X}_{li} \cdot \rho_{FM} \cdot \sigma_{DM})^2} \quad (3.6)$$

Nominal values and variation coefficients (VC) for the BMP of the utilized substrates have been used from [9]. Nominal values and variation coefficients for DM,  $\bar{X}_{pr}$ ,  $\bar{X}_{li}$  and  $\bar{X}_{ash}$  were taken from not yet published ring trial data of DBFZ. Due to the lack of variation coefficients for some substrates, it was assumed that DM,  $\bar{X}_{pr}$ ,  $\bar{X}_{li}$  and  $\bar{X}_{ash}$  had the same variation coefficients for all substrates. The data is reported in Tables 3.1 and 3.2.

Substrate	$\bar{X}_{pr}$ [%DM]	$\bar{X}_{li}$ [%DM]	$\bar{X}_{ash}$ [%DM]	BMP [L/kg FoDM]	DM [%FM]
Grass silage	13.3	2.40	11.1	315.0	31.7
Corn silage	7.81	2.37	4.40	357.0	33.7
Sugar beet silage	3.00	0.19	8.90	657.0	31.8
Cattle manure	16.5	2.48	23.7	230.0	8.08

Table 3.1: Nominal values required for uncertainty propagation computations

Substrate	VC $\bar{X}_{pr}$	VC $\bar{X}_{li}$	VC $\bar{X}_{ash}$	VC $BMP$	VC $DM$
Grass silage	5.223	12.85	17.43	6	2.149
Corn silage	5.223	12.85	17.43	9	2.149
Sugar beet silage	5.223	12.85	17.43	3	2.149
Cattle manure	5.223	12.85	17.43	7	2.149

Table 3.2: Variation coefficients required for uncertainty propagation computations

The resulting probability density functions for all four utilized input substrates as well as the disturbance feeding (see Section 3.2) are depicted in Figure 3.3. Limits for the simulated realizations of inlet concentrations are indicated by blue vertical lines while upper and lower limits used in the multi-stage NMPC scenario formulation (see Section 3.3) are indicated by the colors of the respective substrate.

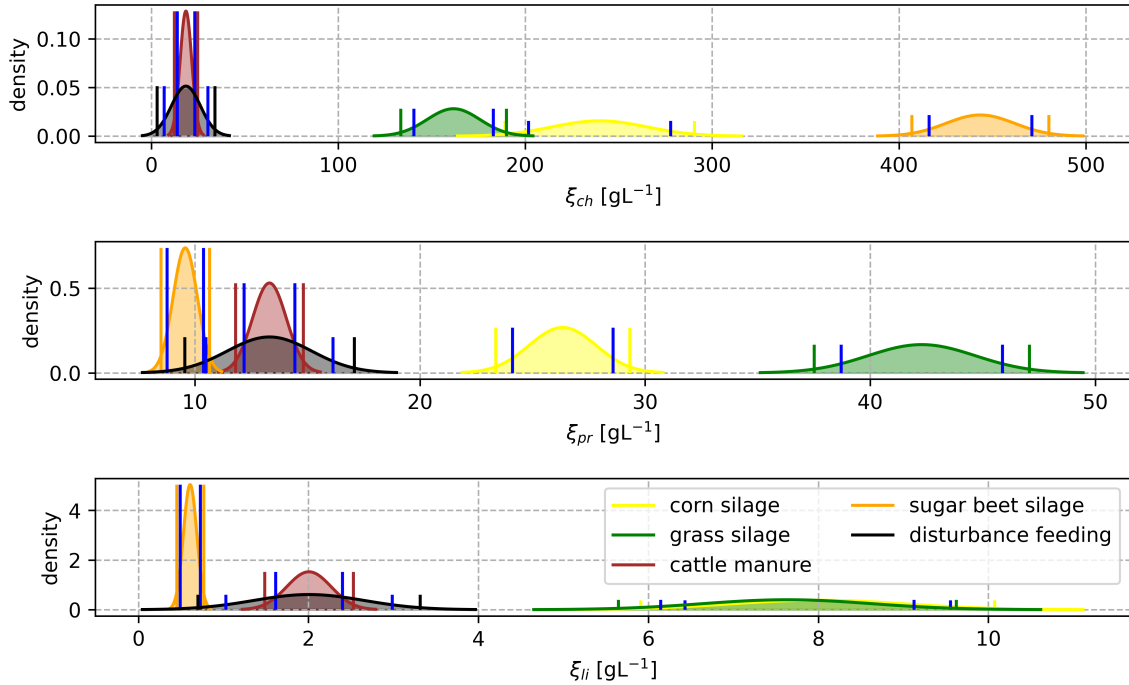


Figure 3.3: Probability density functions for fermentable fractions of macronutrients; vertical lines in color of substrate represent limits used for discrete uncertainty values in multi-stage approach; blue vertical lines represent bounds for simulated values.

## 3.2 Disturbance Feeding

As stated in the introduction, it may be economically beneficial to feed waste products into a biogas plant. In reality this may incorporate the feeding of a certain amount of organic waste into the AD plant over a number of days. Such a situation was simulated in scenario 1b (described later) by dictating the feeding of cattle manure at specified times and volume flow rates into the biogas plant. Therefore, this feeding was fixed and acted as a disturbance rather than an input for the controller. It is therefore referred to as disturbance feeding from now on. The composition of the disturbance cattle manure was impinged with a larger uncertainty to account for the assumption that in reality the composition of such a waste product would most likely not be analyzed but only estimated. Therefore, the standard deviation of its uncertain macronutrients was multiplied by 2.5 as opposed to regular cattle manure.

## 3.3 Multi-stage Scenarios

The goal of the robust multi-stage approach was to ensure robust constraint satisfaction with respect to the gas storage filling level. It was anticipated that these constraints would soonest be violated if the realizations of the uncertain parameter values of the  $\xi_{i,j}$  were at a disadvantageous combination of large positive or negative deviations from their nominal values. This assumption as well as the reports by Lucia and Engel in [21] motivated the modeling of the continuous inlet concentration uncertainties as discrete values at upper and lower bounds. These bounds were set at **two standard deviations** above and below their respective nominal values to cover roughly 95 % of a normal distribution. As stated previously, there were four input substrates as well as one disturbance substrate considered in this thesis. Since each of them contained three macronutrients, this would result in upper and lower discrete uncertainties for a total of 15  $\xi_{i,j}$ , where the index  $i$  refers to the respective macronutrient and  $j$  refers to the respective substrate. Even for robust horizons of one this would lead to  $N_s = 2^{15} = 32,768$  different multi-stage scenarios which was deemed computationally infeasible. Instead, it was decided to group the  $\xi$  values for all macronutrients and vary them simultaneously, e.g.  $\underline{\xi}_{pr} = [\xi_{pr,CS}, \xi_{pr,GS}, \xi_{pr,CM}, \xi_{pr,SBS}, \xi_{pr,disturbing}]$  with  $\underline{\xi}_{pr} \in \{\underline{\xi}_{pr,lower}, \underline{\xi}_{pr,upper}\}$ . This led to a total of  $N_s = 2^3 = 8$  different multi-stage scenarios. The resulting scenario tree is drawn in Figure 3.4 where multi-stage scenarios 1 and 2 as well as 7 and 8 are depicted. The remaining four multi-stage scenarios are indicated by dashed lines.

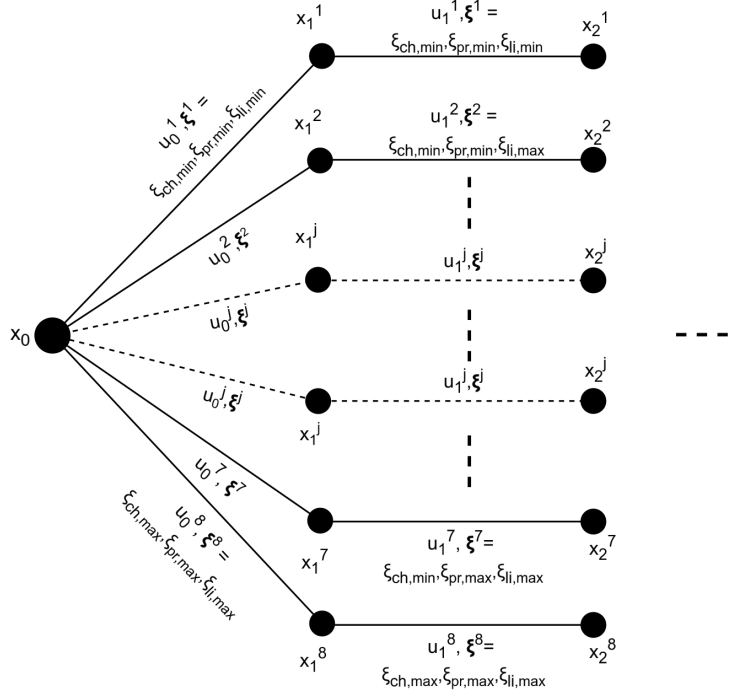


Figure 3.4: Multi-stage scenario tree with robust horizon  $N_r = 1$ .

Robust horizons larger than one were not applied due to the associated exponential growth of the scenario tree and the associated computational costs. Additionally, this choice was motivated by the assumption that realizations of the uncertainties were unknown but approximately constant over time.

### 3.4 Gas Storage Model

A gas storage model was developed as a separate system connected to the digester. The methane ( $CH_4$ ) and carbon-dioxide ( $CO_2$ ) of the gaseous phase of the digester were considered as inflows into the gas storage tank with no return flow allowed. According to [11], biogas produced in the fermenter usually contains water vapor at saturation conditions. As an approximation, the biogas within the tank was therefore also assumed to be always saturated with water vapor ( $H_2O$ ) despite slightly different temperature and pressure. Its resulting partial pressure was computed using the Antoine equation. As gas storages in biogas plants are often partially enclosed by a membrane, the volume of the enclosed gases is variable while the total pressure is approximately constant (isobaric conditions). This was accounted for by a small and constant overpressure of 1 % of atmospheric pressure at standard conditions and making the total volume of the tank variable. The outflow of methane from the tank and into the CHP plant,  $\dot{V}_{CH_4,out}$ , followed the demand of the CHP plant. It was computed separately and could therefore be considered as known. The temperature in the AD

reactor and the tank were assumed to be 311 and 323.25 K. In reality, gas storage temperature is a function of various weather related factors which are in turn dependent on season and daytime as shown by [30]. Pragmatically, the maximum measured temperature in [30] was assumed throughout all corresponding simulations. This leads to a lower, conservative estimation of the actual gas storage capacity.

Two new states were introduced for the filling levels of the main components of the biogas, namely  $x_{19} = V_{\text{CH}_4,\text{tank}}$  and  $x_{20} = V_{\text{CO}_2,\text{tank}}$ . An additional state describing the filling level of water vapor in the tank could be avoided by assuming saturated water vapor in the gas storage.

Expressions for the differential equations of the two filling levels are derived in the following. By assuming a mixture of ideal gases at isobaric conditions, mass balances simplify to volume balances:

$$\dot{V}_{\text{CH}_4,\text{tank}} = \dot{V}_{\text{CH}_4,\text{in}} - \dot{V}_{\text{CH}_4,\text{out}} \quad (3.7\text{a})$$

$$\dot{V}_{\text{CO}_2,\text{tank}} = \dot{V}_{\text{CO}_2,\text{in}} - \dot{V}_{\text{CO}_2,\text{out}}, \quad (3.7\text{b})$$

where 'in' and 'out' indicate volume flows from the digester into the tank and from the tank into the CHP plant, respectively.

Starting with the tank's outflows,  $\dot{V}_{\text{CH}_4,\text{out}}$  can be computed through the demanded electrical power  $P_{\text{elec}}$  at the CHP plant. The mass flow rate of  $\text{CH}_4$  required by the CHP reads

$$\dot{m}_{\text{CH}_4,\text{out}} = \frac{P_{\text{elec}}}{LHV \cdot \eta_{\text{elec}}}, \quad (3.8)$$

with the lower heating value  $LHV$  of  $\text{CH}_4$  and the electrical efficiency of the CHP plant  $\eta_{\text{elec}}$ . With the specific gas constant for methane  $R_{\text{S,CH}_4}$ , this leads to the following equation:

$$\dot{V}_{\text{CH}_4,\text{out}} = \dot{m}_{\text{CH}_4,\text{out}} \cdot R_{\text{S,CH}_4} \cdot \frac{T_{\text{tank}}}{p_{\text{tank}}} = \frac{P_{\text{elec}}}{LHV \cdot \eta_{\text{elec}}} \cdot R_{\text{S,CH}_4} \cdot \frac{T_{\text{tank}}}{p_{\text{tank}}}. \quad (3.9)$$

To compute the outflow of  $\text{CO}_2$  from the tank, a notation commonly found in the thermodynamics community is used. Here,  $y_{\text{CO}_2}$  refers to the volume fraction of  $\text{CO}_2$  with respect to the entire volumetric tank level:

$$y_{\text{CO}_2} = \frac{V_{\text{CO}_2}}{V_{\text{tank}}} = \frac{V_{\text{CO}_2}}{V_{\text{CH}_4} + V_{\text{CO}_2} + V_{\text{H}_2\text{O}}}. \quad (3.10)$$

Analogous notations will be used for the remaining gases.

Under the assumption of an ideal mixture of the gases within the tank, an outflow of  $\dot{V}_{\text{CH}_4,\text{out}}$  leads to the outflow of the remaining gases proportionate to the volume

fraction they take within the tank:

$$\dot{V}_{\text{CO}_2,\text{out}} = \frac{y_{\text{CO}_2}}{1 - y_{\text{CO}_2}} (\dot{V}_{\text{CH}_4,\text{out}} + \dot{V}_{\text{H}_2\text{O},\text{out}}). \quad (3.11)$$

Analogously, this applies to  $\text{H}_2\text{O}$ :

$$\dot{V}_{\text{H}_2\text{O},\text{out}} = \frac{y_{\text{H}_2\text{O}}}{1 - y_{\text{H}_2\text{O}}} (\dot{V}_{\text{CH}_4,\text{out}} + \dot{V}_{\text{CO}_2,\text{out}}). \quad (3.12)$$

Inserting (3.12) into (3.11) leads to (3.13)

$$\dot{V}_{\text{CO}_2,\text{out}} = \frac{\frac{y_{\text{CO}_2}}{1-y_{\text{CO}_2}}}{1 - \frac{y_{\text{CO}_2}y_{\text{H}_2\text{O}}}{(1-y_{\text{CO}_2})(1-y_{\text{H}_2\text{O}})}} \left( \dot{V}_{\text{CH}_4,\text{out}} \left( 1 + \frac{y_{\text{H}_2\text{O}}}{1 - y_{\text{H}_2\text{O}}} \right) \right), \quad (3.13)$$

where the dependence on  $\dot{V}_{\text{H}_2\text{O},\text{out}}$  has been eliminated.

It is now assumed that the pressure and temperature of the volume flow from the AD process into the tank change instantaneously and that the two are directly connected to each other, i.e. there is either no pipe in between the two or the pipe is considered as part of the gas storage from now on. Because of the conservation of mass it is known that the outflow of mass from the AD process  $\dot{m}_g$  must be equal to the inflow of mass into the tank. This is expressed by (3.14).

$$\dot{m}_g = \dot{m}_{\text{tank,in}} \quad (3.14)$$

Inserting the ideal gas law equation and reformulating leads to the following:

$$\dot{V}_{\text{tank,in}} = \dot{V}_g \frac{p_{\text{AD}}}{p_{\text{tank}}} \frac{T_{\text{tank}}}{T_{\text{AD}}}. \quad (3.15)$$

Similarly to the previous consideration, this total volume flow can also be split into the volume flows for the individual gases proportionate to their partial pressures within that volume flow. These partial pressures are known from the ADM1-R3-frac.

Therefore, the following equation holds for the three involved gases indicated by  $i$ .

$$\dot{V}_{i,\text{in}} = \dot{V}_g \frac{p_{\text{AD}}}{p_{\text{tank}}} \frac{T_{\text{tank}}}{T_{\text{AD}}} \frac{p_i}{p_{\text{AD}}}. \quad (3.16)$$

Inserting (3.16) into (3.7a) and (3.7b) leads to the following ordinary differential equations for the two new states:

$$\dot{V}_{\text{CH}_4} = \dot{V}_g \frac{p_{\text{CH}_4}}{p_{\text{tank}}} \frac{T_{\text{tank}}}{T_{\text{AD}}} - \dot{V}_{\text{CH}_4,\text{out}} \quad (3.17a)$$

$$\dot{V}_{\text{CO}_2} = \dot{V}_{\text{g}} \frac{p_{\text{CO}_2}}{p_{\text{tank}}} \frac{T_{\text{tank}}}{T_{\text{AD}}} - \frac{\frac{y_{\text{CO}_2}}{1-y_{\text{CO}_2}}}{1 - \frac{y_{\text{CO}_2}y_{\text{H}_2\text{O}}}{(1-y_{\text{CO}_2})(1-y_{\text{H}_2\text{O}})}} \left( \dot{V}_{\text{CH}_4,\text{out}} \left( 1 + \frac{y_{\text{H}_2\text{O}}}{1-y_{\text{H}_2\text{O}}} \right) \right). \quad (3.17\text{b})$$

Both gas level filling states were normalized to the maximum capacity of the tank. Therefore, the states always assume values between zero and one. However, they typically do not exceed 0.7 since the sum of the two as well as the water vapor volume is constrained to stay within zero and one by the NMPC formulation, see Section 3.8.

## 3.5 Application Scenarios

This research focused on two main application scenarios. Scenario 1 focused on the methanation, i.e. maximum methane production in the AD process for subsequent biogas upgrading and feed-in of purified methane into the natural gas grid. In reality, this would require the separation of  $\text{CO}_2$  from the generated biogas in a biogas upgrader. Since biogas upgrading processes are typically run at steady state, the goal in this scenario was to control the substrate feed such that piecewise constant reference flows of methane are met. The separation of  $\text{CO}_2$  was not modeled. The incorporation of an additional gas storage tank was considered unnecessary as it was assumed that in this scenario the produced biogas flow would be directly fed into the subsequent upgrading process. Additionally, disturbances were to be rejected.

In a second scenario, Scenario 2, the cogeneration process was considered where a CHP plant was included as well as the gas storage model derived in Section 3.4 for buffering purposes.

All sub-scenarios were conducted with time steps of 0.5 h. The set of ordinary differential equations (ODEs) was solved using `do-mpc`'s OCFE implementation with a Gauss-Radau collocation scheme for polynomials of order 2 and one finite element per time step. Prediction and control horizons were always equal as they cannot be set independently of one another in `do-mpc`.

In all sub-scenarios a random uniform feeding error of up to 5% of the computed substrate mass flows was added to simulate imprecise feeding through an auger conveyor or a substrate pump.

### 3.5.1 Scenario 1

The plain normalized ADM1-R3-frac model was used due to the lack of necessity for the gas storage. Three different setpoint changes of methane volume flow were defined, namely 450 to 650, 650 to 550 and 550 to 450  $\text{m}^3 \text{d}^{-1}$ . The setpoint changes were set up for days 3, 6 and 9. These were followed by 21 days of constant operation at a

setpoint of  $450 \text{ m}^3 \text{ d}^{-1}$  of methane production. It shall be noted that the NMPC was not presented with information about upcoming setpoint changes. Thus, the NMPC was not prepared for new setpoints. This resembles real-life scenarios in which sudden, not foreseeable setpoint changes shall be realized.

### **Scenario 1a**

No disturbances were introduced for Scenario 1a.

### **Scenario 1b**

In Scenario 1b the disturbance feeding volume flow rates of a cattle manure were set to  $22.5 \text{ m}^3 \text{ d}^{-1}$  between days 5-10,  $36 \text{ m}^3 \text{ d}^{-1}$  between days 13-17 and  $13.5 \text{ m}^3 \text{ d}^{-1}$  at days 22-26. The feed volume flow rates were known to the controller.

## **3.5.2 Scenario 2**

Scenario 2 covers flexible cogeneration. For this purpose, the ADM1-R3-frac was augmented by the gas storage model described in Section 3.4, thus increasing the total number of ODEs from 18 to 20. Since CHP plants are best operated at maximum capacity due to the resulting best electrical efficiency, the CHP plant was either turned on to 100% capacity or turned off. A weekly operating schedule of the CHP plant was adopted from [24] and repeated for each simulated week. This schedule is laid out in Table 3.3.

Monday	Tuesday	Wednesday	Thursday	Friday	Saturday	Sunday
$07h - 15h$	$07h - 14h$	$07h - 14h$	$07h - 14h$	$07h - 14h$	$09h - 12h$	$00h - 01h$
$16h - 22h$	$15h - 22h$	$16h - 22h$	$15h - 22h$	$16h - 23h$	$17h - 23h$	$11h - 12h$ $17h - 00h$

Table 3.3: CHP operating schedule [24]

### **Scenario 2a**

No disturbances were introduced for scenario 2a.

### **Scenario 2b**

In scenario 2b the disturbance feeding of cattle manure was set to an inlet volume flow of  $4.5 \text{ m}^3 \text{ d}^{-1}$  in between days 5-10.

### Scenario 2c

In scenario 2c, the disturbance feeding from scenario 2b was kept. Additionally, noise was added to the gas storage filling states  $x_{19}$  and  $x_{20}$ . At every time step a random uniform noise of up to  $\pm 1\%$  of the maximum gas storage filling volume was added to each of the two states independently of one another. Every five hours the magnitude of that noise was increased to  $\pm 3\%$  to simulate larger state estimation corrections on a different time scale. In reality this could occur due to different measurement equipment sampling times.

## 3.6 Biogas Plant Dimensioning

Dimensions of the modeled AD plant, gas storage and CHP plant are reported in Table 3.4. The gas storage capacity was taken from [24]. This leads to a ratio of gas storage and CHP capacity of  $5.92 \text{ m}^3 \text{ kW}^{-1}$ , which is slightly larger than the average of  $4.3 \text{ m}^3 \text{ kW}^{-1}$  reported in [5] in 2021.

Parameter	Value
Digester liquid volume	$163 \text{ m}^3$
Digester gas volume	$16.3 \text{ m}^3$
Digester temperature	$311 \text{ K}$
Digester pressure	$1.0133 \text{ bar}$
Digester maximum feed volume flow silage	$80 \text{ m}^3 \text{ d}^{-1}$
Digester maximum feed volume flow manure	$450 \text{ m}^3 \text{ d}^{-1}$
Gas storage volume	$296 \text{ m}^3$ [24]
Gas storage temperature	$323.15 \text{ K}$
Gas storage pressure	$1.0143 \text{ bar}$
CHP electrical capacity	$50 \text{ kW}$
CHP electrical efficiency	$36\%$

Table 3.4: Dimensions of the simulated digester, gas storage and CHP plant

### CHP Plant

For the cogeneration scenario a CHP plant of  $50 \text{ kW}$  electrical capacity with an electrical efficiency of  $36\%$  was used, similar to the  $36.15\%$  of the CHP plant installed at

DBFZ. The required flow rates of  $CH_4$  were computed with a lower heating value of  $50.01 \text{ MJ kg}^{-1}$  and a specific gas constant  $R_{S,CH_4}$  of  $518.4 \text{ J kg}^{-1} \text{ K}^{-1}$  for  $CH_4$  [15].

## 3.7 Simulation Initialization

The simulation of each scenario was preceded by a 300 day open-loop simulation during which a continuous static mix of all four substrates was fed into the AD process to achieve a steady-state within the digester. The mix consisted of  $2/M \text{ m}^3 \text{ d}^{-1}$  of each silage and  $3/M \text{ m}^3 \text{ d}^{-1}$  for the cattle manure with  $M=4$  being the total number of controlled substrates. The larger feeding volume flow for cattle manure was motivated by larger maximum volume flow capacity as reported in Table 3.4.

## 3.8 Cost Functions And Constraints

Since the two scenarios focused on two different tasks, two different cost functions were formulated. The goal of Scenario 1 was to track the setpoints of a reference volume flow of methane from the digester. Therefore, both a stage cost as well as a terminal cost were introduced that penalized the squared deviation of the methane volume outflow of the digester, normalized by the respective setpoint. As stated in Section 3.5.1, all setpoints within the moving horizon of the NMPC remained at the current setpoint up until a setpoint change. The stage cost weight  $c_1$  was tuned for quick adjustment to new setpoints, while the terminal cost weight  $c_2$  was tuned for small permanent control errors. Additionally, the input of substrates was penalized proportionate to their respective cost, which was implemented as a stage cost term. Both a linear and a quadratic input cost formulation were tested. This term was added to incentivize an economic substrate usage. Initial tests also showed that the addition of another cost term was required which penalized the squared change of individual feed inputs over consecutive time steps. This prevented the controller from acting too erratically which often led to a non-recoverable drop in pH value, in the pH range of 4-5.

As stated in Section 2.1.1, inputs as well as states have been normalized which simplified their consideration in the cost function. The normalized inputs were constrained between 0 and 1. With the exception of state 14 which represents the residual free ion concentration, all other states had to remain strictly positive due to their physical meaning. Enforcing this through constraints proved to be unnecessary during initial tests, which is why the state constraints  $x_i > 0 \quad \forall i \in \{1, \dots, 18\} \setminus \{14\}$  were dropped. The resulting cost function for Scenario 1 is shown in (3.18). The stated linear and a quadratic input costs are denoted by the power  $l \in \{1, 2\}$ . The system of nonlinear ODEs, which describe the AD process and are discretized by OCFE, are denoted

in the system matrix  $\mathbf{F}$ . Measurements reflected in the measurement equation pose additional constraints to the optimization problem.

$$\begin{aligned} \min_{\underline{u}} \quad J(\underline{x}, \underline{u}) = & c_1 \cdot \sum_{k=0}^{N_c-1} \left( \left( \frac{\dot{V}_{\text{CH}_4, \text{AD}, k+1} - \dot{V}_{\text{CH}_4, \text{AD}, k+1, \text{set}}}{\dot{V}_{\text{CH}_4, \text{AD}, k+1, \text{set}}} \right)^2 \right) \\ & + c_2 \cdot \left( \frac{\dot{V}_{\text{CH}_4, \text{AD}, N_c} - \dot{V}_{\text{CH}_4, \text{AD}, N_c, \text{set}}}{\dot{V}_{\text{CH}_4, \text{AD}, N_c, \text{set}}} \right)^2 \\ & + \sum_{k=0}^{N_c-1} \sum_{i=1}^M \left( c_3 \cdot \Delta u_{i,k}^2 + \frac{\text{cost}_i}{\text{cost}_{\max}} \cdot u_{i,k}^l \right) \end{aligned} \quad (3.18)$$

$$\text{subject to } \underline{x}_{k+1} = \mathbf{F}(\underline{x}_k, \underline{u}_k)$$

$$\underline{y}_k = \mathbf{H}(\underline{x}_k)$$

$$u_{i,k} \in [0, 1] \quad \forall \quad i \in \{1, \dots, 4\}, k \in \{0, \dots, N_c\}$$

$$l \in \{1, 2\}$$

For both Scenario 1a and 1b, the same cost function coefficients were applied which are reported in Table 3.5.

Coefficient	Value
$c_1$	10
$c_2$	100
$c_3$	0.1

Table 3.5: Cost function coefficients Scenario 1

The goal of Scenario 2 was to ensure a gas storage filling volume within the specified bounds during flexible operation of the CHP plant. Therefore, unlike in Scenario 1, no setpoints were to be tracked. Instead, a cost function inspired by [24] was formulated which penalized the squared deviation of the gas filling from a optimal filling percentage over the entire control horizon. The gas storage's deviation from it was additionally penalized by the power of four to increase the steepness of the resulting deviation function close to the lower and upper limit of the gas storage. After initial tests at 50% optimal filling level, better results were achieved at lower optimal filling levels. By trial and error an optimal filling level of 43% was found. The normalized gas storage filling itself was computed by the sum of its individual normalized components,  $x_{19}$ ,  $x_{20}$  and  $\frac{V_{\text{H}_2\text{O,tank}}}{V_{\max,\text{tank}}}$ . The weights  $c_1$  and  $c_2$  were tuned by trial and error. A substrate cost term was added for the same reason as stated above. Since initial tests indicated no necessity for the penalization of the input change, this cost term was neglected for Scenario 2.

In addition to the input constraints described for Scenario 1, the gas storage states

$x_{19}$  and  $x_{20}$  were constrained to be positive.

The normalized gas storage filling was also constrained between 5% and 95% with the addition of slack variables  $\epsilon_i$  to soften the constraints.

The formulated cost function of Scenario 2, described in (3.19), represents the cost function for a single multi-stage scenario. The entire cost function used in this multi-stage NMPC formulation consisted of the summation of all eight multi-stage scenario cost functions at equal weights and is not displayed.

System and measurement equations are once again additional constraints to the optimization problem. As opposed to Scenario 1, the system of ODEs now contains an additional two equations for the gas storage filling level states.

$$\begin{aligned}
 \min_{\underline{u}, \epsilon_1, \epsilon_2} \quad & J(\underline{x}, \underline{u}) = \sum_{k=0}^{N_c-1} \left( c_1 \cdot \left( x_{19,k} + x_{20,k} + \frac{V_{H_2O, tank, k+1}}{V_{max, tank}} - 0.43 \right)^2 \right. \\
 & \quad \left. + c_2 \cdot \left( x_{19,k} + x_{20,k} + \frac{V_{H_2O, tank, k+1}}{V_{max, tank}} - 0.43 \right)^4 \right) \\
 & \quad + \sum_{k=0}^{N_c-1} \sum_{i=1}^M \frac{cost_i}{cost_{max}} \cdot u_{i,k}^l + c_3 \cdot (\epsilon_1 + \epsilon_2) \\
 \text{subject to} \quad & \underline{x}_{k+1} = \mathbf{F}(\underline{x}_k, \underline{u}_k) \\
 & \underline{y}_k = \mathbf{H}(\underline{x}_k) \\
 & u_{i,k} \in [0, 1] \quad \forall \quad i \in \{1, \dots, 4\}, k \in \{0, \dots, N_c\} \\
 & l \in \{1, 2\} \\
 & x_{19,k}, x_{20,k} \geq 0 \quad \forall \quad k \in \{0, \dots, N_c\} \\
 & \left( x_{19,k} + x_{20,k} + \frac{V_{H_2O, tank, k+1}}{V_{max, tank}} \right) - \epsilon_1 \leq 0.95 \quad \forall \quad k \in \{0, \dots, N_c\} \\
 & \left( x_{19,k} + x_{20,k} + \frac{V_{H_2O, tank, k+1}}{V_{max, tank}} \right) - \epsilon_2 \leq -0.05 \quad \forall \quad k \in \{0, \dots, N_c\} \\
 & \epsilon_m \in [0, 0.05] \quad \forall \quad m \in \{1, 2\}
 \end{aligned} \tag{3.19}$$

For all sub-scenarios of Scenario 2, the same cost function coefficients were applied which are reported in Table 3.6.

Coefficient	Value
$c_1$	0.5
$c_2$	50
$c_3$	10

Table 3.6: Cost function coefficients Scenario 2

The shape of the designed cost function for any time index  $k$  within the control horizon is displayed in Figure 3.5 with respect to the gas storage filling level. The quadratic filling level term as well as the effect of the slack variables above or below the soft constraints, indicated by dashed blue lines, play a minor role in comparison to the filling level term raised by the power of four. Note that the inputs are neglected here but would each contribute at a magnitude between 0 and 1 depending on their relative cost and feed volume flow rate.

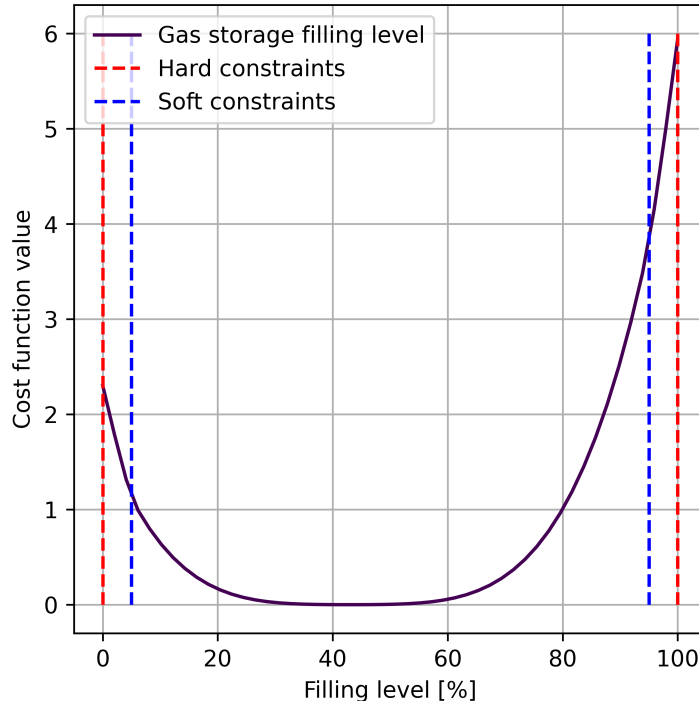


Figure 3.5: Cost function shape for Scenario 2 with respect to filling level.

## 3.9 Software

This software for this research was implemented in Python 3.10.12. The code has been designed in an object-oriented manner with several abstractions that are described in

more detail in Appendix A.4. Additionally, UML diagrams for both the classes as well as the packages are provided.

The open-source library `do-mpc`, version 4.6.4, was utilized as a framework for the Model Predictive Control implementation, both for nominal and multi-stage applications. Model definitions defined through `do-mpc`, like the ADM1-R3-frac in this case, are automatically represented as CasADi symbolic functions [4] and variables by `do-mpc` [12]. IPOPT [37] is used by `do-mpc` as a non-linear solver. Acceleration of the nonlinear solver is enabled through the embedding of the faster linear solver MA27 of the Coin-HSL library [2].

The software design of the conducted research shall not be described in detail but the UML diagrams for classes and package structure are depicted in Figures A.13, A.14 and A.15 in Appendix A.4.

The simulations were conducted on a 64-bit Ubuntu 22.04.03 LTS system with an Intel i9-9900K CPU and 32GB RAM.

# 4 Results and Discussion

In the following the results from both simulated scenarios are presented and discussed. It shall be noted that all displayed inputs,  $u_{\text{feed,silage}}$  or  $u_{\text{feed,manure}}$  respectively, display the actual feed volume flows into the AD plant per time step (0.5 h). Since they are affected by the random errors described in Section 3.5, they may exceed their limit  $u_{\max}$  by up to 5 %. Their upper limit, displayed by a dashed red line, refers to both axes, i.e. to silages and manure.

This chapter also covers a discussion on runtime analysis and controller stability as well as limitations of this thesis.

## 4.1 Methanation

Initially, different control horizons were tested for Scenario 1a with a linear substrate cost formulation. Starting with  $N_c = 5$  and incrementing at steps of 5, a control horizon of  $N_c = 15$  was found to lead to satisfactory tracking. Horizon lengths in numbers of time steps and absolute lengths are reported in Table 4.1.

Horizon	Number of time steps [-]	Time [h]
Prediction horizon $N_p$	15	7.5
Control horizon $N_c$	15	7.5
Robust horizon $N_r$	0	0

Table 4.1: Horizon lengths applied to Scenario 1

However, it was observed that the step response to setpoint changes led to pointy progressions of the generated methane volume flow  $\dot{V}_{\text{CH}_4}$  as displayed around days 3, 6 and 9 in Figure 4.6. It was also observed that the setpoint value increase at day 3 was met by the feeding of mainly sugar beet silage, which in terms of macronutrients mainly consists of carbohydrates. This substrate composition in turn allows for a faster conversion to biogas as compared to a composition of mainly lipid-rich substrates as is the case with cattle manure. A significant usage of this substrate by the NMPC algorithm was observed when setpoint values were lowered such as on days 6 and 9.

A permanent control error of less than 1% remained approximately one day after the final setpoint change. The displayed input variables  $u_{\text{feed,silage}}$  and  $u_{\text{feed,manure}}$  represent the computed values which were then subjected to the random feeding errors before being applied in the plant simulation. It could be observed that the NMPC controller took these disturbances into account by considering the input variables which fluctuated slightly even during steady-state operation as displayed in the magnification during days 15-25.

Relatively large drops of pH value in between -0.18 and -0.1 were observed at any of the setpoint changes, regardless of the predominantly fed substrate(s). Recovery to previous pH value levels either did not occur due to highly frequent setpoint changes or it took place within one or two days after each setpoint change. During the steady-state operation in between days 9 and 30 the pH value leveled out at approximately 7.24.

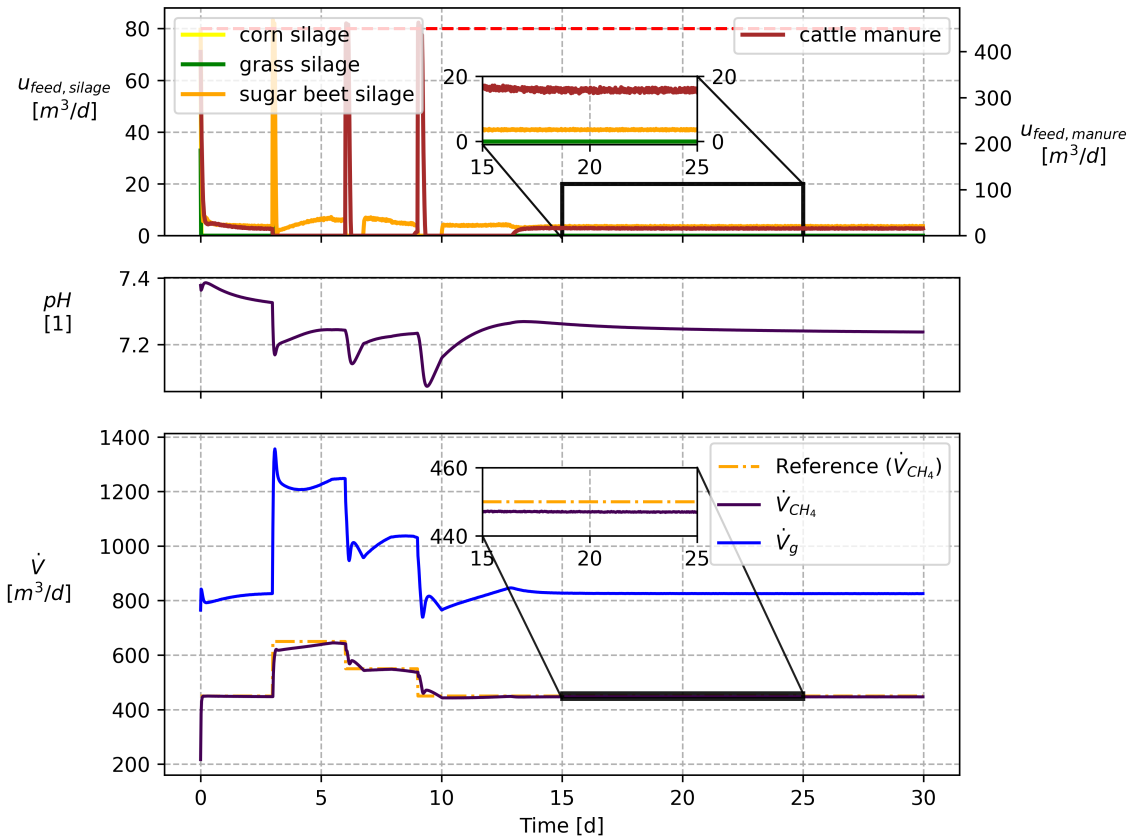


Figure 4.6: Scenario 1a: Setpoint tracking of generated methane volume flow with  $N_c = 15$  and linear penalization of substrate costs. Slow and pointy step responses exhibited. Steady-state controller inputs and setpoint tracking displayed in the magnification.

Subsequently, the usage of a quadratic substrate cost formulation was tested again for Scenario 1a with the same control horizon  $N_c = 15$ . Response to setpoint changes

appeared similar to first-order behavior, and a negligible permanent control error was observed within less than one day after the respective setpoint changes. Additionally, substrates were fed in smaller quantities at a time which led to smaller drops in the pH value of the AD plant.

The overall usage of substrates was significantly lower both immediately after set-point changes as well as during steady-state operation. In this formulation, the steady-state methane generation was almost solely accomplished through the feeding with cheap cattle manure at  $\sim 9 \text{ m}^3 \text{ d}^{-1}$ . By contrast, in the linear formulation cattle manure had been fed at  $\sim 18 \text{ m}^3 \text{ d}^{-1}$  and  $\sim 3 \text{ m}^3 \text{ d}^{-1}$  of the more expensive sugar beet silage while still achieving worse control performance.

Due to the lower feeding volume flow during steady-state operation, the pH value also recovered to higher values of  $\sim 7.33$  during this time, compared with  $\sim 7.24$  for the linear substrate cost penalization.

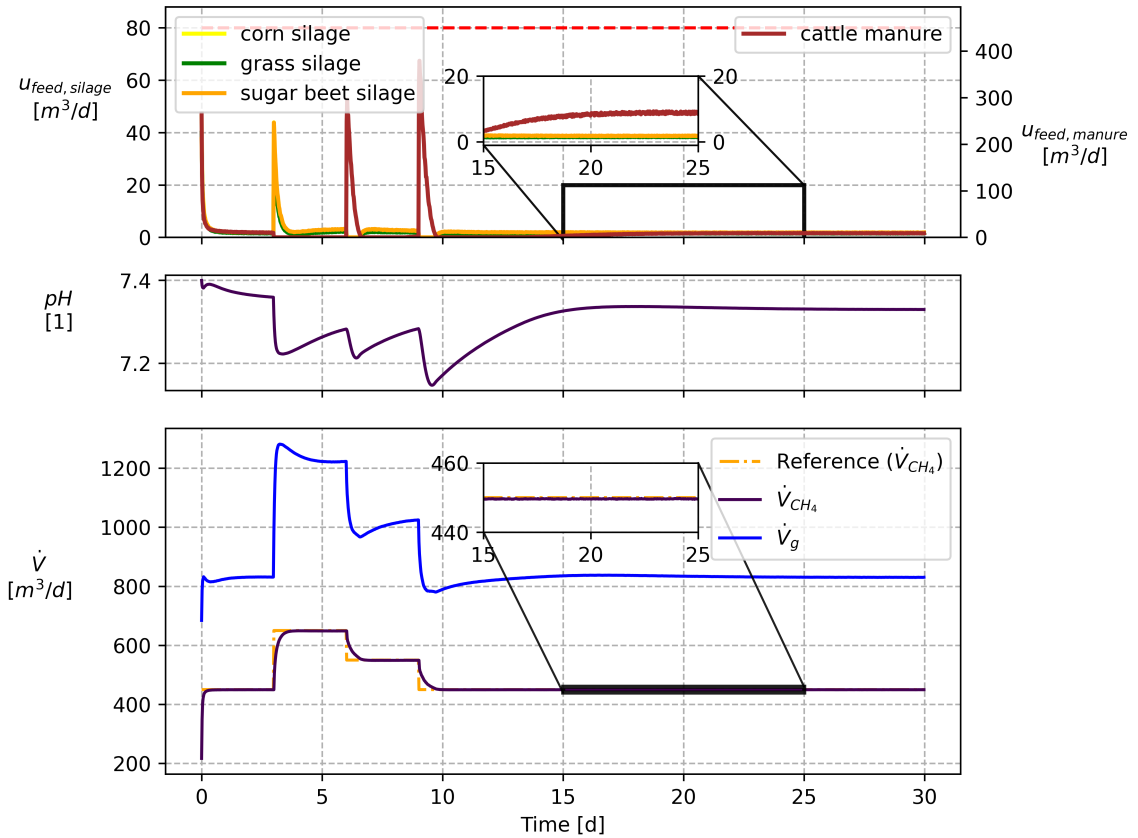


Figure 4.7: Scenario 1a: Setpoint tracking of generated methane volume flow with  $N_c = 15$  and quadratic penalization of substrate costs. Quick step responses without overshoot is exhibited. Steady-state controller inputs and setpoint tracking displayed in the magnification.

The NMPC with the control parameters from Scenario 1a was then tested on Scenario 1b, where volume flows of cattle manure with large uncertainty were introduced

as disturbances. Due to the large disturbance feed volume flows, the pH values were observed to drop significantly at times. The NMPC could not prevent this due to the lack of a buffer solution as an input. However, after the end of each disturbance, the pH values did recover.

The setpoint tracking in the first ten days, where multiple setpoint changes were superimposed with a disturbance feeding, showed similar behavior as in the previous sub-scenario without the disturbance. A small control error was observed in between days 13 and 17 where the steady-state operation was disturbed by the largest disturbance feeding with small spikes in the methane generation at the beginning and at the end of the disturbance period. The controller countered this disturbance by feeding silages as displayed in the magnification region of the inputs. While the generation of methane could be continued during this period, it can be assumed that a continued disturbance of this magnitude could not be sustained by this controller due to the lack of a buffer solution. Consequently, the continued drop in pH could not be prevented, which would lead to inhibition after a few more days. Results are displayed in Figure 4.8.

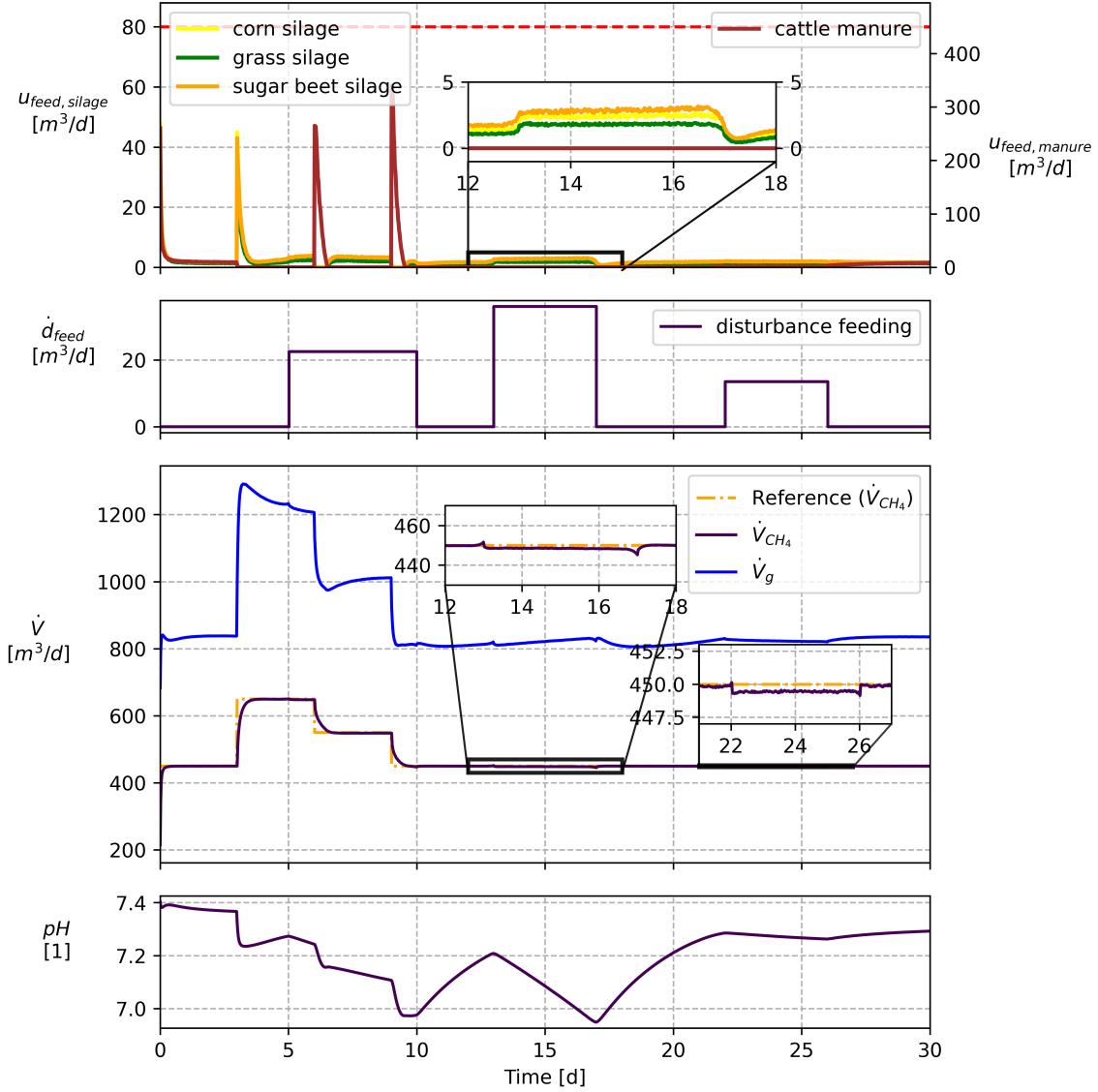


Figure 4.8: Scenario 1b: Setpoint tracking of generated methane volume flow with  $N_c = 15$  and quadratic penalization of substrate costs.  $22.5 \text{ m}^3 \text{ d}^{-1}$  of disturbance feeding added between days 5 and 10. Disturbance rejection is displayed in the magnification.

## 4.2 Cogeneration

The schedule of the CHP plant exhibited large daily variations in demand for methane. For example, the CHP plant operated 9 h on Sunday, followed by 14 h on Monday. This required a rapid increase in biogas production on Monday mornings while the CHP operating time of Friday night was followed by a lengthy 10 h period of no methane demand. It was therefore anticipated that unlike in Scenario 1, the controller in Scenario 2 would require longer control horizons to be able to foresee methane demand

sufficiently far into the future. This assumption was supported by initial tests in which controllers with control horizons of 20-30 time steps (10 to 15 h) were not able to satisfy the gas storage constraints.

Therefore, a control horizon of 40 time steps (20 h) was chosen which could look further ahead than the longest down times of the CHP plant. Moreover, in a real-life application the fixed, known CHP schedule would most likely be replaced by predicted CHP schedules, the accuracy of which naturally declines with longer prediction horizons. This assumption represented another motivation for the chosen control horizon. The robust horizon was chosen at 1 as motivated in Section 3.3. All horizons used in this scenario are reported in Table 4.2.

Horizon	Number of time steps [-]	Time [h]
Prediction horizon $N_p$	40	20
Control horizon $N_c$	40	20
Robust horizon $N_r$	1	0.5

Table 4.2: Horizon lengths applied to Scenario 2

To present the results of the simulation studies in Scenario 2, relevant states and variables are depicted in Figures 4.9 - 4.11. These include the feed volume flows  $u_{\text{feed,silage}}$  and  $u_{\text{feed,manure}}$ , gas storage fill levels of  $CH_4$  and  $CO_2$  with respect to the total gas storage capacity, the total gas storage fill level, biogas and methane production rates as well as the AD process' pH value. Figures 4.10 and 4.11 additionally display the disturbance feeding. Soft constraints are depicted as dashed blue lines whereas hard constraints are depicted as dashed red lines.

Simulation results of Scenario 2a are depicted in Figure 4.9 by means of additional subplots related to the gas storage filling levels as opposed to the plots in Scenario 1. In all subplots weekly repeating patterns could be observed for weeks 2-4. In contrast to that, distinctly different courses were observed in week 1, especially in the feeding inputs as well as the resulting biogas and methane production rates. Methane and total biogas production rates  $\dot{V}_{CH_4,AD}$  and  $\dot{V}_{g,AD}$  were higher in week 1 as compared to the following weeks. Thus, it was concluded that the average biogas production had to be decreased by the controller. This was supported by four distinct feeding spikes in cattle manure within days 0-4 which had previously been identified to be one of the mechanisms of the controller to slow down biogas production.

Although both the  $CH_4$  and  $CO_2$  filling levels started out at 20 % with respect to the gas storage capacity, a difference between the two states quickly emerged. For the remainder of the simulation the  $CH_4$  filling level was larger than the  $CO_2$  filling level.

This was most prominent at times of high gas storage filling levels during the first 8 days after which the difference decreased again.

The total gas storage filling level was on average below 50 % as designed by the cost function formulation in (3.19). Feeding pauses of more than two days were observed, starting slightly before the weekends which decreased biogas production rates significantly. Still, a noticeable increase in all gas storage filling levels could be observed during those times due to the shorter CHP operating times accompanied by the non-negligible remaining biogas production rates.

Compliance with all imposed constraints was observed, namely the lower hard constraints of 0 % for the tank filling level states as well as the total tank filling level constraints.

With regards to AD process stability, the pH value started slightly below 7.3 and increased gradually during the first 5 days. It subsequently stabilized around 7.4 for the remainder of the simulation while dropping occasionally due to feeding intervals. Overall, the AD process once again appeared to be stable.

In between days 0-4 the NMPC commanded for three large feeding spikes in cattle manure. It was assumed that this was due to a high total volume flow of biogas  $\dot{V}_{g,AD}$  after the steady state simulation at  $\sim 400 \text{ m}^3 \text{ d}^{-1}$  combined with arbitrarily set initial fill levels of  $CH_4$  and  $CO_2$  in the gas storage. Feeding a large volume of cattle manure helped decreasing  $\dot{V}_{g,AD}$ , thus staying well within the constraints of the gas storage. It could be observed that in line with expectations the gas storage fill level increased around days 6-7, 13-14, 20-21 and 27-28 due to shorter operating times of the CHP plant on the weekends. The control horizon of 20 hours (or 40 time steps) allowed the NMPC to foresee the drop in demand for  $CH_4$  and pause feeding of the AD plant on Fridays.

Volume flows of  $CH_4$  varied in between  $130$  and  $320 \text{ m}^3 \text{ d}^{-1}$ , indicating a very flexible production of biogas.

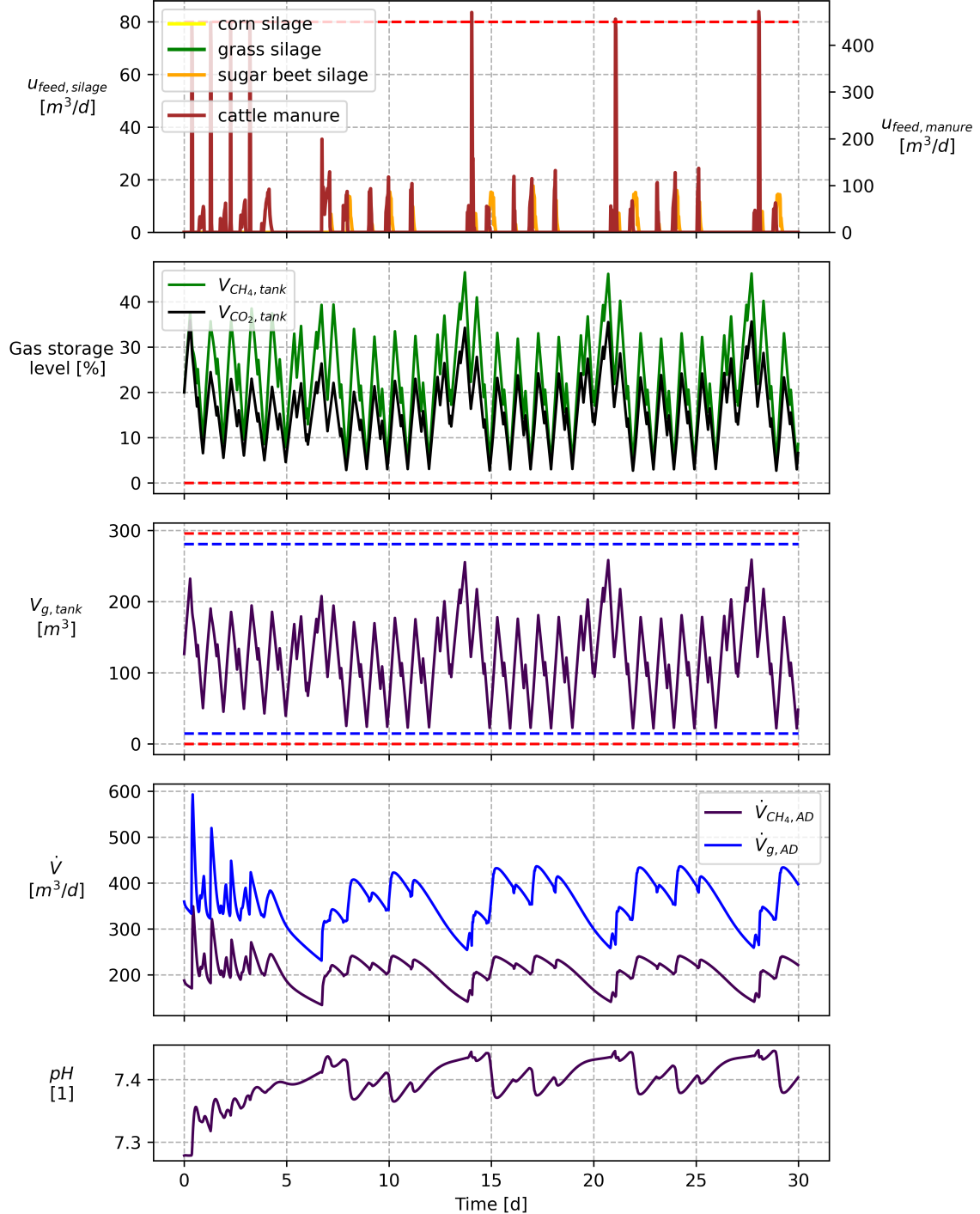


Figure 4.9: Scenario 2a: CHP schedule tracking with added gas storage and multi-stage approach with  $N_c = 40$ ,  $N_r = 1$ . Maximum substrate feedings differ between silages and manure. Stable AD process without gas storage constraint violations was observed.

As opposed to Scenario 2a, two additional cattle manure feeding spikes were observed at day 4 and day 7 as shown in Figure 4.10. While the spike at day 4 could not be explained, the spike at day 7 was attributed to the rejection of the disturbance

feeding. Pulse feeding of cattle manure was previously described as a mechanism used by the controller to temporarily break biogas production. However, the continued disturbance feeding of cattle manure during days 5-10, which was significantly smaller than in Scenario 1b, slightly increased biogas production rates. The total gas storage filling level on day 7 is therefore noticeably increased when compared to Scenario 2a. Therefore, either the steep increase in the cost function close to the gas storage limit or the proximity to the soft constraint presumably triggered the temporary braking mechanism of pulse feeding of cattle manure.

Weeks 2-4 displayed very similar controller and plant behavior as in Scenario 2a. It was therefore concluded that the disturbance feeding did not destabilize the plant due to its relatively small volume flow. Overall, no constraint violations were observed.

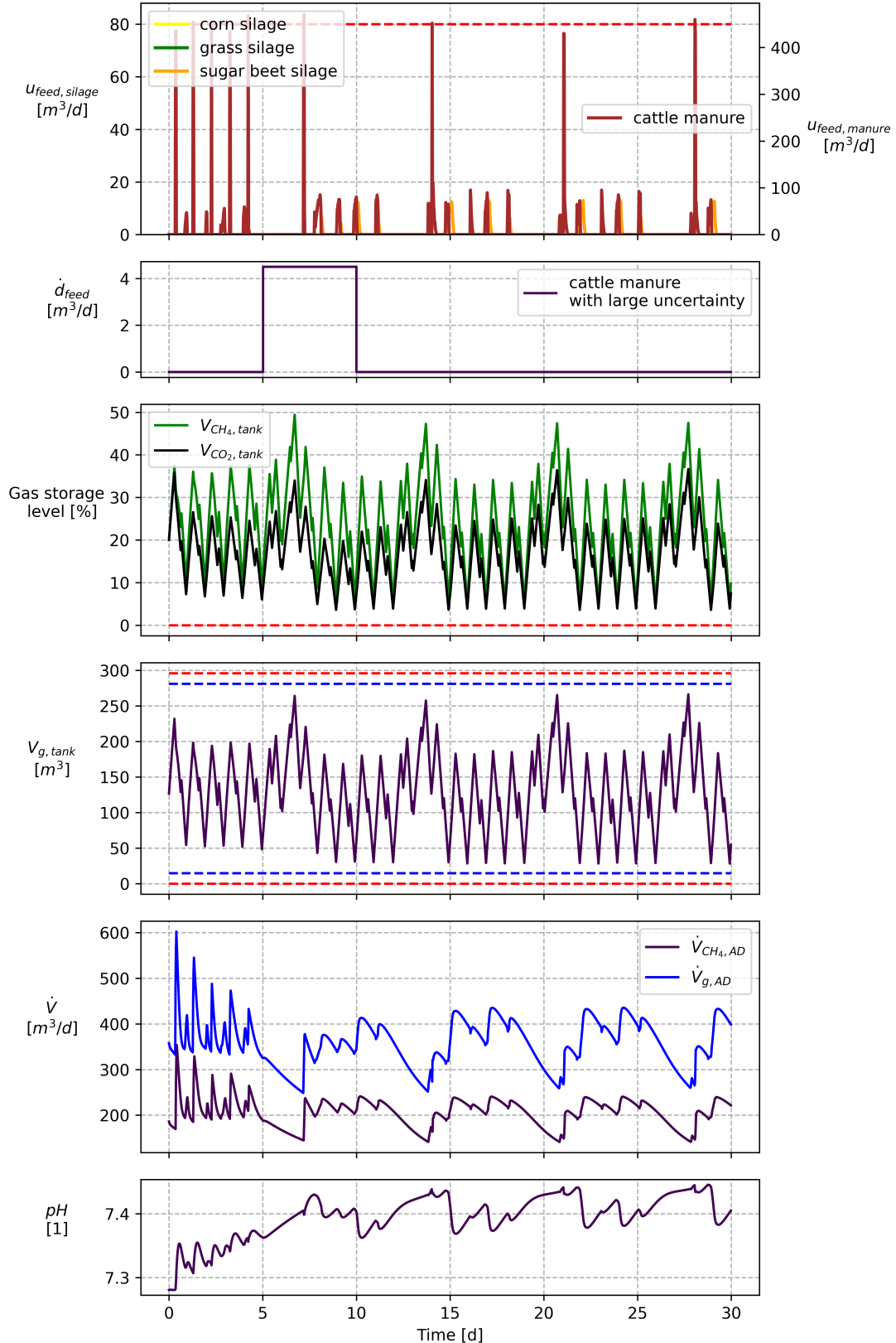


Figure 4.10: Scenario 2b: CHP schedule tracking with added gas storage and multi-stage approach with  $N_c = 40$ ,  $N_r = 1$ .  $22.5 \text{ m}^3 \text{ d}^{-1}$  of disturbance feeding was added between days 5 and 10. Maximum substrate feedings differ between silages and manure. Stable AD process without gas storage constraint violations was observed.

The AD plant behavior in Scenario 2c was very similar to Scenario 2b throughout the entire simulation as displayed in Figure 4.11. However, the controller acted significantly more erratic with more medium sized spikes of both sugar beet silage and cattle manure. This was attributed to the noise introduced to the estimation of the gas storage states (not displayed). Therefore, the controller foresaw constraint violations more frequently and responded accordingly.

The more erratic feeding inputs seemed to only slightly alter the course of the biogas production rates which can be perceived in the more pointed biogas production rates.

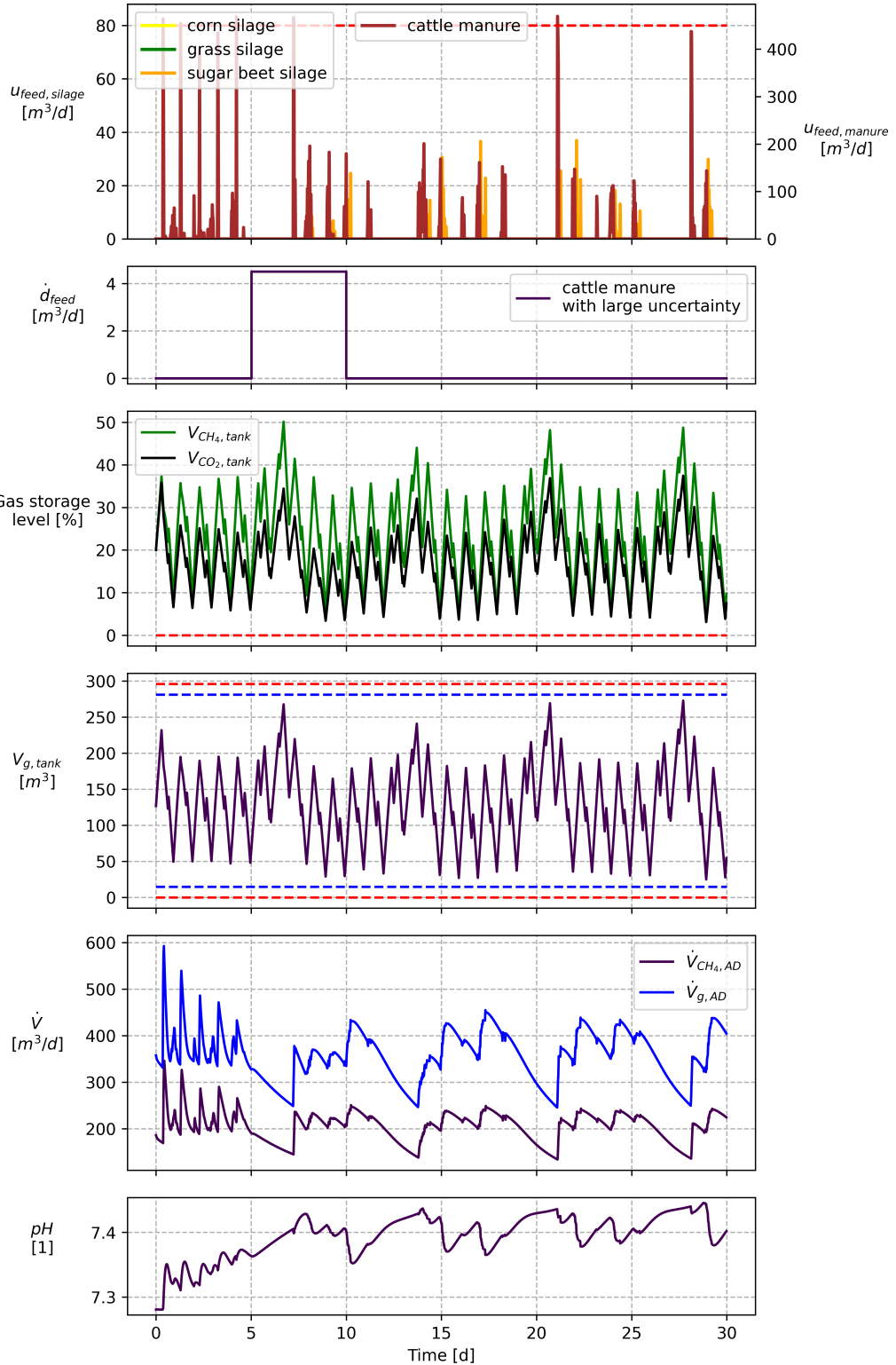


Figure 4.11: Scenario 2c: CHP schedule tracking with added gas storage with noise added to estimated gas storage states (not depicted). Multi-stage approach with  $N_c = 40$ ,  $N_r = 1$ .  $22.5 \text{ m}^3 \text{ d}^{-1}$  of disturbance feeding was added between days 5 and 10. Maximum substrate feedings differ between silages and manure. Stable AD process without gas storage constraint violations was observed.

In all three sub-scenarios of Scenario 2, the controller almost solely used cattle manure and sugar beet silage while neglecting the other two available substrates, grass silage and corn silage. As opposed to the other two silages, sugar beet silage consisted of a significantly larger carbohydrate concentration and was used for rapid increases of biogas production rates whereas cattle manure was fed for the opposite reason. Usage of other substrates could be incentivized by altering relative substrate costs in future studies.

Additionally, it was concluded that the controller was able to increase the biogas production rate significantly faster than to decrease it without compromising on AD process stability. Therefore, research on the usage of other substrates or buffer solutions as inputs is encouraged to create a more effective braking mechanism for biogas production rates. This could lead to the successful employment of flexible cogeneration strategies with even smaller gas storage tanks.

### 4.3 Runtime Analysis

The runtimes of individual NMPC iterations were measured and analyzed for all five scenarios. The boxplot in Figure 4.12 depicts the results of this analysis. The displayed data was extracted from the controllers that achieved the best results for their respective scenario. Since the controllers for Scenario 1 featured no robust horizon and had a significantly shorter control horizon of  $N_c = 15$  as compared to the control horizon of  $N_c = 40$  for Scenario 2, both the average and maximum runtimes were significantly lower. Additionally, the implemented gas storage model contributed to longer runtimes due to the increased number of differential equations in Scenario 2 as well as the added constraints. Adding disturbance feeding did not show a negative effect on the runtimes as can be seen in similar means and percentiles of the runtimes for the respective sub-scenarios 1a and 1b as well as 2a and 2b. Noise in the estimation of the gas storage fill states  $x_{19}$  and  $x_{20}$  in Scenario 2c was expected to lead the controller close to an infeasible state. However, its aversion did not lead to longer NMPC iterations. In all five sub-scenarios a noticeable spread of runtimes above the 75th percentile was observed. These significantly above average runtimes were attributed to more complex NMPC iterations, e.g. around setpoint changes (Scenario 1), changes in disturbance feedings or the gas storage filling level close to a constraint. Surprisingly, the longest runtime was observed in Scenario 2a rather than the more complex scenarios 2b and 2c at 48.97 s. As even this longest observed iteration time was more than 30 times shorter than the NMPC time step of 0.5 hours, it was concluded that the application of the designed controllers is real-time capable even on a computing platform less potent than the one used in this study.

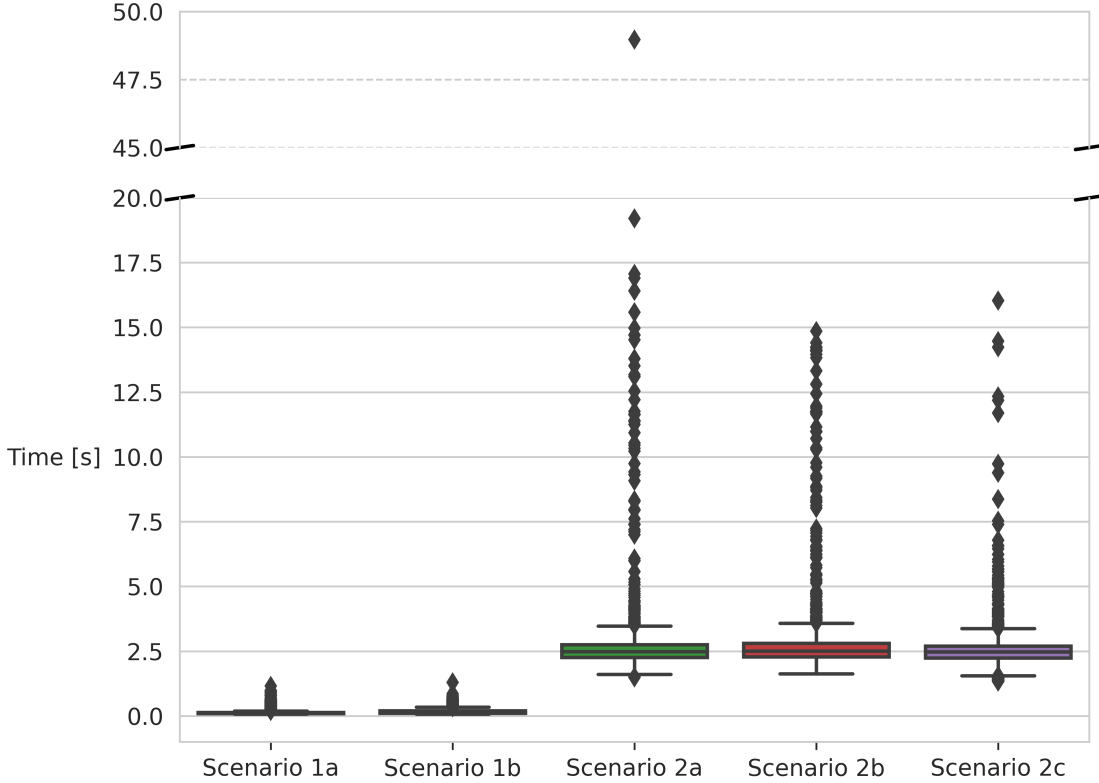


Figure 4.12: Boxplot of NMPC iteration runtimes in seconds; mean and variance of run-times in Scenario 2 significantly larger than in Scenario 1

## 4.4 Controller Stability

Another important aspect when designing a controller is its stability analysis. Lucia et al. [23] have demonstrated guaranteed Input-to-State stability for multi-stage NMPC formulations. However, these proofs were based on the fulfillment of certain assumptions, some of which were not met by the multi-stage NMPC formulation used in this thesis. The most important one that was not met relates to the realizations of the considered uncertainties. These must only assume the values described in the scenario-tree [23]. This is not the case in this study because the uncertain inlet concentrations not only can take any value in between the discrete considered limits but also with a marginal probability values outside those limits.

It is important to note that although Input-to-State stability could not be theoretically proven, this does not mean that the designed controllers were unstable. On the contrary, no indicators of instability such as sustained or growing oscillations could be observed in the conducted simulations. Additionally, in Scenario 1 the setpoint tracking was achieved without overshoot and marginal permanent control error.

## 4.5 Limitations and Assumptions

This work was limited to simulation studies only. Further, the plant-model mismatch was restricted to different realizations of the inlet concentrations in between the controller and the simulated AD plant. More specifically, these differences were assumed to exist for the macronutrient composition of the substrates. Some additional assumptions were introduced which included the assumption of statistical independence of the uncertain parameters required for the uncertainty propagation in Section 3.1.2.

With regards to the process parameters, it was assumed that the kinetic constants, the temperatures in the digester and in the gas storage as well as the gas storage's pressure remained constant throughout the simulation. Lastly, state feedback was assumed in this thesis, i.e. the direct measurement of all states of the plant. Some of them cannot be measured online or at all in reality while the online measurement of others would be financially infeasible due to cost associated with required measurement equipment. The implementation of soft sensors represents a possible alternative and is set out briefly in Chapter 6.



## 5 Theses

- Nominal NMPC is sufficiently robust for the methanation scenario with present substrate uncertainties.
- Multistage NMPC framework is capable to control substrate feed to maintain stable operating conditions.
- Penalization of weighted square of input changes is required to prevent the biogas plant from becoming too acidic in the methanation scenario.
- NMPC applied cattle manure input mainly for temporary limitation or reduction of methane gas production, while applying the silage substrates for quick increase in methane production.
- Random feeding errors have negligible impact on control performance.
- The limited capability to decrease the biogas production rate restricts the minimum gas storage size.
- An extensible software framework was developed which allows for integration of state observers, application on real biogas plant, etc.
- Real time application of designed NMPC controllers is possible.
- The integration of a soft sensor is required for real life application.
- Further research on fermentation quotients of non-agricultural substrates is required for application in the presented control scheme.



## 6 Extended Conclusions and Outlook

Nonlinear Model Predictive Controllers have been developed to control the substrate feeding of a biogas plant for two different application scenarios. The goal of the first application scenario was to track setpoints of methane volume flow rates. The second scenario covered the flexible generation of biogas according to the schedule of a CHP plant. A gas storage model was developed for this scenario to simulate gas storage buffering. Thus, the controller had to satisfy the storage capacity constraints.

The developed controllers were tested in simulations of their respective scenarios under the assumption of state feedback. Both controllers were shown to successfully control the AD plants in their respective scenario. Several introduced disturbances were satisfactorily rejected. These included feed control errors, dictated substrate feeds with increased uncertainty in their macronutrient composition, as well as jumps in the gas storage fill level states.

Uncertainties in the macronutrient composition of the utilized substrates were considered. Under the assumptions laid out in Section 4.5, the realistically scaled uncertainties did not lead to the violation of gas storage fill constraints even in the highly dynamic schedule of the connected CHP plant. This was attributed to the usage of a multi-stage NMPC formulation that considered eight different multi-stage scenarios of macronutrient compositions. Additionally, the nominal NMPC scheme applied to Scenario 1 was shown to also successfully deal with those uncertainties. It was therefore concluded that in case of state feedback macronutrient composition uncertainties do not have a significant impact on control performance.

The usage of an elaborate process model based on the ADM1-R3 [35] allowed for the evaluation of the AD process stability which has often been neglected by the models used for similar tasks in the literature as in [24]. The controller proposed in this reference was tested under similar conditions to Scenario 2 of this thesis, but with a simpler gas storage model and without the consideration of macronutrient uncertainties. They were able to achieve a better ratio of CHP plant electrical capacity to gas storage size. On the other hand, a PI controller proposed by Raeyatdoost et al. [28] had a significantly worse CHP power to gas storage ratio than in this thesis.

Run time analyses of the NMPC computations indicated feasibility for real-time control for time steps of 0.5 h. To address the previously described problem of non-measurable

states, it is planned to implement an observer, e.g. using Moving Horizon Estimation (MHE) or some version of a Kalman Filter. Hellmann et al. [18] have examined various Unscented Kalman Filter (UKF) designs for an anaerobic digestion plant. Although applied to a different simplified version of the ADM1, their findings may also hold for the ADM1-R3-frac. Further, Subramanian et al. [31] demonstrated the feasibility of coupling a multi-stage NMPC controller with an UKF where robust constraint satisfaction was achieved.

It is suggested to study economic aspects of the proposed control design. Although substrate costs have been considered in the cost functions, no computations were conducted to examine the overall profit and loss statement with the inclusion of generated revenues at the electricity price exchange.

It is conceivable that in a real-life scenario CHP schedules might show significantly larger variations in day to day operation. For instance, a sunny and windy week may lead to little to no economic incentives for CHP operation over the duration of multiple days due to other renewable energy sources being cheaper. In this case the developed controllers would most likely not be able to maintain the gas storage filling level below maximum capacity because the AD process cannot be slowed down sufficiently without endangering plant stability. It will therefore be necessary to develop economically sensible strategies for such instances based on mechanisms like methane flaring or other transitional usage of the generated biogas to free up space in the gas storage.

# Bibliography

- [1] *Collection of methods for biogas Methods to determine parameters for analysis purposes and parameters that describe processes in the biogas sector*, DBFZ Deutsches Biomasseforschungszentrum gemeinnützige GmbH, Leipzig. 2nd edition edition. 2020. OCLC: 1338637350.
- [2] HSL, a collection of Fortran codes for large-scale scientific computation. See <https://www.hsl.rl.ac.uk/>. Technical report. Feb. 2024.
- [3] V. ALCARAZ-GONZÁLEZ, F. A. FREGOSO-SÁNCHEZ, V. GONZÁLEZ-ALVAREZ, and J.-P. STEYER: Multivariable Robust Regulation of Alkalinities in Continuous Anaerobic Digestion Processes: Experimental Validation. In: *Processes*, Bd. 9(7), S. 1153, July 2021.
- [4] J. A. E. ANDERSSON, J. GILLIS, G. HORN, J. B. RAWLINGS, and M. DIEHL: CasADi: a software framework for nonlinear optimization and optimal control. In: *Mathematical Programming Computation*, Bd. 11(1), S. 1–36, Mar. 2019.
- [5] T. BARCHMANN, M. POHL, V. DENYSENKO, E. FISCHER, J. HOFMANN, M. LENHART, J. POSTEL, J. LIEBETRAU, and F. N. ROHSTOFFE (Hrsg.): *Biogas-Messprogramm III*, Fachagentur Nachwachsende Rohstoffe e.V. (FNR), Gülzow-Prüzen. Erstausgabe edition. 2021.
- [6] D. BATSTONE, J. KELLER, I. ANGELIDAKI, S. KALYUZHNYI, S. PAVLOSTATIS, A. ROZZI, W. SANDERS, H. SIEGRIST, and V. VAVILIN: The IWA Anaerobic Digestion Model No 1 (ADM1). In: *Water Science and Technology*, Bd. 45(10), S. 65–73, May 2002.
- [7] L. T. BIEGLER: Nonlinear programming strategies for dynamic chemical process optimization. In: *Theoretical Foundations of Chemical Engineering*, Bd. 48(5), S. 541–554, Sept. 2014.
- [8] K. DADHE and S. ENGELL: Robust nonlinear model predictive control: A multi-model nonconservative approach. In: *Book of Abstracts, Int. Workshop on NMPC, Pavia*. Bd. 24. 2008.

- [9] V. DANDIKAS, C. HERRMANN, B. HÜLSEMANN, and H. OECHSNER: *Gasausbeute in landwirtschaftlichen Biogasanlagen: Potenziale, Erträge, Einflussfaktoren*, 526 in KTBL-Schrift, Kuratorium für Technik und Bauwesen in der Landwirtschaft e.V. (KTBL), Darmstadt. 2021.
- [10] S. L. DE OLIVEIRA: *Model Predictive Control (MPC) for Constrained Nonlinear Systems*. Dissertation, California Institute of Technology, Jan. 2008.  
Medium: PDF Version Number: Final.
- [11] C. DIECKMANN, W. EDELMANN, M. KALTSCHMITT, J. LIEBETRAU, S. OLDENBURG, M. RITZKOWSKI, F. SCHOLWIN, H. STRÄUBER, and S. WEINRICH: Biogaserzeugung und -nutzung. In: M. KALTSCHMITT, H. HARTMANN, and H. HOFBAUER (Hrsg.): *Energie aus Biomasse*, S. 1609–1755, Springer Berlin Heidelberg, Berlin, Heidelberg. 2016.
- [12] F. FIEDLER, B. KARG, L. LÜKEN, D. BRANDNER, M. HEINLEIN, F. BRABENDER, and S. LUCIA: do-mpc: Towards FAIR nonlinear and robust model predictive control. In: *Control Engineering Practice*, Bd. 140, S. 105676, Nov. 2023.
- [13] B. A. FINLAYSON: Orthogonal collocation on finite elements—progress and potential. In: *Mathematics and Computers in Simulation*, Bd. 22(1), S. 11–17, Mar. 1980.
- [14] D. GAIDA, C. WOLF, and M. BONGARDS: Feed control of anaerobic digestion processes for renewable energy production: A review. In: *Renewable and Sustainable Energy Reviews*, Bd. 68, S. 869–875, Feb. 2017.
- [15] K.-H. GROTE and J. FELDHUSEN (Hrsg.): *Dubbel: Taschenbuch für den Maschinenbau*, Springer Berlin Heidelberg, Berlin, Heidelberg. 2011.
- [16] J. GÜSEWELL, M. HÄRDITLEIN, and L. ELTROP: A plant-specific model approach to assess effects of repowering measures on existing biogas plants: The case of Baden-Wuerttemberg. In: *GCB Bioenergy*, Bd. 11(1), S. 85–106, Jan. 2019.
- [17] T. A. N. HEIRUNG, J. A. PAULSON, J. O’LEARY, and A. MESBAH: Stochastic model predictive control — how does it work? In: *Computers & Chemical Engineering*, Bd. 114, S. 158–170, June 2018.
- [18] S. HELLMANN, T. WILMS, S. STREIF, and S. WEINRICH: Comparison of Unscented Kalman Filter Design for Agricultural Anaerobic Digestion Model, 2023. Publisher: arXiv Version Number: 3.

- [19] H. H. KU and OTHERS: Notes on the use of propagation of error formulas. In: *Journal of Research of the National Bureau of Standards*, Bd. 70(4), 1966.
- [20] LEI XUE, DEWEI LI, and YUGENG XI. Nonlinear model predictive control of anaerobic digestion process based on reduced ADM1. In: *2015 10th Asian Control Conference (ASCC)*. S. 1–6. Kota Kinabalu. May 2015 IEEE.
- [21] S. LUCIA and S. ENGELL. Control of towing kites under uncertainty using robust economic nonlinear model predictive control. In: *2014 European Control Conference (ECC)*. S. 1158–1163. Strasbourg, France. June 2014 IEEE.
- [22] S. LUCIA, T. FINKLER, and S. ENGELL: Multi-stage nonlinear model predictive control applied to a semi-batch polymerization reactor under uncertainty. In: *Journal of Process Control*, Bd. 23(9), S. 1306–1319, Oct. 2013.
- [23] S. LUCIA, S. SUBRAMANIAN, D. LIMON, and S. ENGELL: Stability properties of multi-stage nonlinear model predictive control. In: *Systems & Control Letters*, Bd. 143, S. 104743, Sept. 2020.
- [24] E. MAUKY, S. WEINRICH, H. NÄGELE, H. F. JACOBI, J. LIEBETRAU, and M. NELLES: Model Predictive Control for Demand-Driven Biogas Production in Full Scale. In: *Chemical Engineering & Technology*, Bd. 39(4), S. 652–664, Apr. 2016.
- [25] H. O. MÉNDEZ-ACOSTA, B. PALACIOS-RUIZ, V. ALCARAZ-GONZÁLEZ, J.-P. STEYER, V. GONZÁLEZ-ÁLVAREZ, and E. LATRILLE: Robust Control of Volatile Fatty Acids in Anaerobic Digestion Processes. In: *Industrial & Engineering Chemistry Research*, Bd. 47(20), S. 7715–7720, Oct. 2008.
- [26] E. R. PICENO-DÍAZ, L. A. RICARDEZ-SANDOVAL, M. A. GUTIERREZ-LIMON, H. O. MÉNDEZ-ACOSTA, and H. PUEBLA: Robust Nonlinear Model Predictive Control for Two-Stage Anaerobic Digesters. In: *Industrial & Engineering Chemistry Research*, Bd. 59(52), S. 22559–22572, Dec. 2020.
- [27] J. POHLODEK, H. ALSMEIER, B. MORABITO, C. SCHLAUCH, A. SAVCHENKO, and R. FINDEISEN: Stochastic Model Predictive Control Utilizing Bayesian Neural Networks, 2023. Publisher: arXiv Version Number: 1.
- [28] N. RAEYATDOOST, R. ECCLESTON, and C. WOLF: Flexible Methane Production Using a Proportional Integral Controller with Simulation-Based Soft Sensor. In: *Chemical Engineering & Technology*, Bd. 43(1), S. 75–83, Jan. 2020.

- [29] D. SCHRÖER and U. LATACZ-LOHMANN: Flexibilization or biomethane upgrading? Investment preference of German biogas plant operators for the follow-up of guaranteed feed-in tariffs. In: *GCB Bioenergy*, Bd. 16(2), S. e13111, Feb. 2024.
- [30] M. STUR, M. POHL, C. KREBS, and E. MAUKY: Charakterisierung von Biogasspeichern: Einflüsse und Methodenvergleich. In: *LANDTECHNIK*, S. Bd. 77 Nr. 1 (2022), Mar. 2022. Publisher: LANDTECHNIK.
- [31] S. SUBRAMANIAN, S. LUCIA, and S. ENGELL: Economic Multi-stage Output Feedback NMPC using the Unscented Kalman Filter. In: *IFAC-PapersOnLine*, Bd. 48(8), S. 38–43, 2015.
- [32] A. TAWAI and M. SRIARIYANUN: Nonlinear Optimization-Based Robust Control Approach for a Two-Stage Anaerobic Digestion Process. In: P. L. GENTILI (Hrsg.): *Journal of Chemistry*, Bd. 2022, S. 1–18, July 2022.
- [33] S. WEINRICH: Practical modelling of biogas plantsPraxisnahe Modellierung von Biogasanlagen, 2018. Publisher: Universität Rostock.
- [34] S. WEINRICH, E. MAUKY, T. SCHMIDT, C. KREBS, J. LIEBETRAU, and M. NELLES: Systematic simplification of the Anaerobic Digestion Model No. 1 (ADM1) – Laboratory experiments and model application. In: *Bioresource Technology*, Bd. 333, S. 125104, Aug. 2021.
- [35] S. WEINRICH and M. NELLES: Systematic simplification of the Anaerobic Digestion Model No. 1 (ADM1) – Model development and stoichiometric analysis. In: *Bioresource Technology*, Bd. 333, S. 125124, Aug. 2021.
- [36] F. WEISSBACH: Die Bewertung von nachwachsenden Rohstoffen für die Biogasgewinnung. In: *Teil I: Das Gasbildungspotenzial der fermentierbaren Nährstoffe. Pflanzenbauwissenschaften*, Bd. 13(2), S. 72–85, 2009.
- [37] A. WÄCHTER and L. T. BIEGLER: On the implementation of an interior-point filter line-search algorithm for large-scale nonlinear programming. In: *Mathematical Programming*, Bd. 106(1), S. 25–57, Mar. 2006.

# Appendix

## A.1 Normalized Equations of ADM1-R3-frac

The normalization notation is laid out for states  $x$ , inputs  $u$  and outputs  $y$ . All normalization matrices  $\mathbf{T}_i$  are diagonal matrices. Their entries are comprised of the corresponding vectors and are reported for  $\mathbf{T}_x$  and  $\mathbf{T}_u$  in Section A.3.2. As the normalization of  $\mathbf{T}_y$  is arbitrary, its entries are not reported.

$$\underline{x} = \mathbf{T}_x \bar{x}, \quad (.1a)$$

$$\underline{y} = \mathbf{T}_y \bar{y}, \quad (.1b)$$

$$\underline{u} = \mathbf{T}_u \bar{u}, \quad (.1c)$$

where  $\bar{x}$ ,  $\bar{y}$ , and  $\bar{u}$  are the normalized coordinates. Accordingly, inlet concentrations are normalized with the same matrix as the states, resulting in

$$\underline{\xi} = \mathbf{T}_x \bar{\xi}. \quad (.2)$$

Normalized state differential equations:

$$\begin{aligned} \dot{\bar{x}}_1 &= c_1 (\bar{\xi}_1 - \bar{x}_1) T_u \bar{u} + a_{1,1}\theta_1 \frac{T_{x,6}}{T_{x,1}} \bar{x}_6 + a_{1,2}\theta_2 \frac{T_{x,7}}{T_{x,1}} \bar{x}_7 + a_{1,3}\theta_3 \frac{T_{x,8}}{T_{x,1}} \bar{x}_8 + \\ &\quad a_{1,4}\theta_4 \frac{T_{x,9}}{T_{x,1}} \bar{x}_9 - a_{1,5}\theta_6 T_{x,11} \frac{\bar{x}_1 \bar{x}_{11}}{\theta_7 + T_{x,1} \bar{x}_1} \bar{I}_{ac} \end{aligned} \quad (.3a)$$

$$\begin{aligned} \dot{\bar{x}}_2 &= c_1 (\bar{\xi}_2 - \bar{x}_2) T_u \bar{u} + a_{2,1}\theta_1 \frac{T_{x,6}}{T_{x,2}} \bar{x}_6 + a_{2,2}\theta_2 \frac{T_{x,7}}{T_{x,2}} \bar{x}_7 + a_{2,3}\theta_3 \frac{T_{x,8}}{T_{x,2}} \bar{x}_8 + \\ &\quad a_{2,4}\theta_4 \frac{T_{x,9}}{T_{x,2}} \bar{x}_9 + a_{2,5}\theta_6 \frac{T_{x,1} T_{x,11}}{T_{x,2}} \frac{\bar{x}_1 \bar{x}_{11}}{\theta_7 + T_{x,1} \bar{x}_1} \bar{I}_{ac} - c_5 \bar{x}_2 + c_6 \frac{T_{x,17}}{T_{x,2}} \bar{x}_{17} \end{aligned} \quad (.3b)$$

$$\begin{aligned} \dot{\bar{x}}_3 &= c_1 (\bar{\xi}_3 - \bar{x}_3) T_u \bar{u} + a_{3,1}\theta_1 \frac{T_{x,6}}{T_{x,3}} \bar{x}_6 + a_{3,2}\theta_2 \frac{T_{x,7}}{T_{x,3}} \bar{x}_7 + a_{3,3}\theta_3 \frac{T_{x,8}}{T_{x,3}} \bar{x}_8 - \\ &\quad a_{3,4}\theta_4 \frac{T_{x,9}}{T_{x,3}} \bar{x}_9 + a_{3,5}\theta_6 \frac{T_{x,1} T_{x,11}}{T_{x,3}} \frac{\bar{x}_1 \bar{x}_{11}}{\theta_7 + T_{x,1} \bar{x}_1} \bar{I}_{ac} - c_5 \bar{x}_3 + c_5 \frac{T_{x,15}}{T_{x,3}} \bar{x}_{15} + \\ &\quad c_7 \frac{T_{x,18}}{T_{x,3}} \bar{x}_{18} \end{aligned} \quad (.3c)$$

$$\dot{\bar{x}}_4 = c_1 (\bar{\xi}_4 - \bar{x}_4) T_u \bar{u} - a_{4,1}\theta_1 \frac{T_{x,6}}{T_{x,4}} \bar{x}_6 - a_{4,2}\theta_2 \frac{T_{x,7}}{T_{x,4}} \bar{x}_7 + a_{4,3}\theta_3 \frac{T_{x,8}}{T_{x,4}} \bar{x}_8 -$$

$$a_{4,4}\theta_4 \frac{T_{x,9}}{T_{x,4}}\bar{x}_9 - a_{4,5}\theta_6 \frac{T_{x,1} T_{x,11}}{T_{x,4}} \frac{\bar{x}_1 \bar{x}_{11}}{\theta_7 + T_{x,1}\bar{x}_1} \bar{I}_{\text{ac}} \quad (.3d)$$

$$\begin{aligned} \dot{\bar{x}}_5 &= c_1 \left( \bar{\xi}_5 - \bar{x}_5 \right) T_u \bar{u} - a_{5,1}\theta_1 \frac{T_{x,6}}{T_{x,5}} \bar{x}_6 - a_{5,2}\theta_2 \frac{T_{x,7}}{T_{x,5}} \bar{x}_7 - a_{5,3}\theta_3 \frac{T_{x,8}}{T_{x,5}} \bar{x}_8 - \\ &\quad a_{5,4}\theta_4 \frac{T_{x,9}}{T_{x,5}} \bar{x}_9 + a_{5,5}\theta_6 \frac{T_{x,1} T_{x,11}}{T_{x,5}} \frac{\bar{x}_1 \bar{x}_{11}}{\theta_7 + T_{x,1}\bar{x}_1} \bar{I}_{\text{ac}} \end{aligned} \quad (.3e)$$

$$\dot{\bar{x}}_6 = c_1 \left( \theta_9 \bar{\xi}_6 - \bar{x}_6 \right) T_u \bar{u} - \theta_1 \bar{x}_6 + a_{6,6}\theta_5 \frac{T_{x,10}}{T_{x,6}} \bar{x}_{10} + a_{6,7}\theta_5 \frac{T_{x,11}}{T_{x,6}} \bar{x}_{11} \quad (.3f)$$

$$\dot{\bar{x}}_7 = c_1 \left( (1 - \theta_9) \frac{T_{x,6}}{T_{x,7}} \bar{\xi}_6 - \bar{x}_7 \right) T_u \bar{u} - \theta_2 \bar{x}_7 \quad (.3g)$$

$$\dot{\bar{x}}_8 = c_1 \left( \bar{\xi}_8 - \bar{x}_8 \right) T_u \bar{u} - \theta_3 \bar{x}_8 + a_{8,6}\theta_5 \frac{T_{x,10}}{T_{x,8}} \bar{x}_{10} + a_{8,7}\theta_5 \frac{T_{x,11}}{T_{x,8}} \bar{x}_{11} \quad (.3h)$$

$$\dot{\bar{x}}_9 = c_1 \left( \bar{\xi}_9 - \bar{x}_9 \right) T_u \bar{u} - \theta_4 \bar{x}_9 + a_{9,6}\theta_5 \frac{T_{x,10}}{T_{x,9}} \bar{x}_{10} + a_{9,7}\theta_5 \frac{T_{x,11}}{T_{x,9}} \bar{x}_{11} \quad (.3i)$$

$$\begin{aligned} \dot{\bar{x}}_{10} &= c_1 \left( \bar{\xi}_{10} - \bar{x}_{10} \right) T_u \bar{u} + a_{10,1}\theta_1 \frac{T_{x,6}}{T_{x,10}} \bar{x}_6 + a_{10,2}\theta_2 \frac{T_{x,7}}{T_{x,10}} \bar{x}_7 + \\ &\quad + a_{10,3}\theta_3 \frac{T_{x,8}}{T_{x,10}} \bar{x}_8 + a_{10,4}\theta_4 \frac{T_{x,9}}{T_{x,10}} \bar{x}_9 - \theta_5 \bar{x}_{10} \end{aligned} \quad (.3j)$$

$$\dot{\bar{x}}_{11} = c_1 \left( \bar{\xi}_{11} - \bar{x}_{11} \right) T_u \bar{u} + \theta_6 T_{x,1} \frac{\bar{x}_1 \bar{x}_{11}}{\theta_7 + T_{x,1}\bar{x}_1} \bar{I}_{\text{ac}} - \theta_5 \bar{x}_{11} \quad (.3k)$$

$$\dot{\bar{x}}_{12} = c_1 \left( \bar{\xi}_{12} - \bar{x}_{12} \right) T_u \bar{u} \quad (.3l)$$

$$\dot{\bar{x}}_{13} = c_1 \left( \bar{\xi}_{13} - \bar{x}_{13} \right) T_u \bar{u} \quad (.3m)$$

$$\dot{\bar{x}}_{14} = c_{29} \left( \frac{T_{x,1}}{T_{x,14}} \bar{x}_1 - \bar{x}_{14} \right) - c_9 \bar{x}_{14} \bar{S}_{\text{H}^+} \quad (.3n)$$

$$\dot{\bar{x}}_{15} = c_{30} \left( \frac{T_{x,3}}{T_{x,15}} \bar{x}_3 - \bar{x}_{15} \right) - c_{10} \bar{x}_{15} \bar{S}_{\text{H}^+} \quad (.3o)$$

$$\dot{\bar{x}}_{16} = c_{31} \left( \frac{T_{x,4}}{T_{x,16}} \bar{x}_4 - \bar{x}_{16} \right) - c_{11} \bar{x}_{16} \bar{S}_{\text{H}^+} \quad (.3p)$$

$$\begin{aligned} \dot{\bar{x}}_{17} &= c_{22} T_{x,17}^2 \bar{x}_{17}^3 + c_{23} T_{x,17} T_{x,18} \bar{x}_{17}^2 \bar{x}_{18} + c_{24} T_{x,18}^2 \bar{x}_{17} \bar{x}_{18}^2 + c_{25} T_{x,17} \bar{x}_{17}^2 + \\ &\quad + c_{26} T_{x,18} \bar{x}_{17} \bar{x}_{18} + c_{12} \frac{T_{x,2}}{T_{x,17}} \bar{x}_2 + c_{27} \bar{x}_{17} \end{aligned} \quad (.3q)$$

$$\begin{aligned} \dot{\bar{x}}_{18} &= c_{24} T_{x,18}^2 \bar{x}_{18}^3 + c_{23} T_{x,17} T_{x,18} \bar{x}_{17} \bar{x}_{18}^2 + c_{22} T_{x,17}^2 \bar{x}_{17}^2 \bar{x}_{18} + c_{26} T_{x,18} \bar{x}_{18}^2 + \\ &\quad + c_{25} T_{x,17} \bar{x}_{17} \bar{x}_{18} + c_{12} \frac{T_{x,3}}{T_{x,18}} \bar{x}_3 - c_{12} \frac{T_{x,15}}{T_{x,18}} \bar{x}_{15} + c_{28} \bar{x}_{18} \end{aligned} \quad (.3r)$$

Therein,  $\bar{I}_{\text{ac}}$  and  $\bar{S}_{\text{H}^+}$  are defined as

$$\bar{I}_{\text{ac}} = \frac{c_3}{c_3 + \bar{S}_{\text{H}^+}^{c_2}} \frac{\bar{x}_4}{\bar{x}_4 + c_8/T_{x,4}} \frac{\theta_8}{\theta_8 + T_{x,16}\bar{x}_{16}} \quad (.4)$$

$$\bar{S}_{\text{H}^+} = -\frac{\bar{\Phi}}{2} + \frac{1}{2} \sqrt{\bar{\Phi}^2 + c_4}, \text{ where} \quad (.5)$$

$$\bar{\Phi} = T_{x,13} \bar{x}_{13} + \frac{T_{x,4} \bar{x}_4 - T_{x,16} \bar{x}_{16}}{17} - \frac{T_{x,15} \bar{x}_{15}}{44} - \frac{T_{x,14} \bar{x}_{14}}{60}. \quad (.6)$$

Normalized measurements:

$$\begin{aligned}\bar{y}_1 = \dot{V}_g &= c_{13} \frac{T_{x,17}^2}{T_{y,1}} \bar{x}_{17}^2 + c_{14} \frac{T_{x,17} T_{x,18}}{T_{y,1}} \bar{x}_{17} \bar{x}_{18} + c_{15} \frac{T_{x,18}^2}{T_{y,1}} \bar{x}_{18}^2 + c_{16} \frac{T_{x,17}}{T_{y,1}} \bar{x}_{17} + \\ &+ c_{17} \frac{T_{x,18}}{T_{y,1}} \bar{x}_{18} + \frac{c_{18}}{T_{y,1}}\end{aligned}\quad (.7a)$$

$$\bar{y}_2 = p_{\text{ch4}} = c_{19} \frac{T_{x,17}}{T_{y,2}} \bar{x}_{17} \quad (.7b)$$

$$\bar{y}_3 = p_{\text{co2}} = c_{20} \frac{T_{x,18}}{T_{y,3}} \bar{x}_{18} \quad (.7c)$$

$$\bar{y}_4 = pH = -T_{y,4}^{-1} \log_{10} \bar{S}_{\text{H}^+} \quad (.7d)$$

$$\bar{y}_5 = S_{\text{IN}} = \frac{T_{x,4}}{T_{y,5}} \bar{x}_4 \quad (.7e)$$

$$\bar{y}_6 = TS = T_{y,6}^{-1} \left( 1 - \frac{T_{x,5}}{c_{21}} \bar{x}_5 \right) \quad (.7f)$$

$$\bar{y}_7 = VS = T_{y,7}^{-1} \left( 1 - \frac{T_{x,12}}{c_{21} - T_{x,5} \bar{x}_5} \bar{x}_{12} \right) \quad (.7g)$$

$$\bar{y}_8 = S_{\text{ac}} = \frac{T_{x,1}}{T_{y,8}} \bar{x}_1 \quad (.7h)$$

## A.2 State Vector

Table A.1: Description of state vector components

State	Description
$S_{ac}$	Acetic acid - dissolved
$S_{ch4}$	Methane - dissolved
$S_{IC}$	Inorganic carbon - dissolved
$S_{IN}$	Inorganic nitrogen
$S_{h2o}$	Water
$X_{ch,f}$	Carbohydrates - fast processing
$X_{ch,s}$	Carbohydrates - slow processing
$X_{pr}$	Proteins
$X_{li}$	Lipids
$X_{bac}$	Residual microbial biomass
$X_{ac}$	Microbial biomass of acetoclastic methanogens
$X_{ash}$	Ash
$S_{ion}$	Residual free ions
$S_{ac^-}$	Dissociated acetic acid
$S_{hco3^-}$	Hydrogen carbonate
$S_{nh3}$	Ammonia
$S_{ch4,gas}$	Methane - gaseous
$S_{co2,gas}$	Carbon dioxide - gaseous

## A.3 Parameters

### A.3.1 Substrates

Table A.2: Values of inlet concentrations ' $\xi$ ' [ $\text{g L}^{-1}$ ]

	corresponding state	corn silage	grass silage	sugar beet silage	manure	disturbance feeding
$\xi_1$	$S_{\text{ac}}$	10.32	10.44	8.17	4.535	4.535
$\xi_4$	$S_{\text{IN}}$	0.764	1.574	0.07	1.303	1.303
$\xi_5$	$S_{\text{h2o}}$	662.714	682.59	607.254	919.16	919.16
$\xi_6$	$X_{\text{ch,f}}$	239.754	161.633	443.448	18.468	18.468
$\xi_8$	$X_{\text{pr}}$	26.334	42.283	9.573	13.313	13.313
$\xi_9$	$X_{\text{li}}$	7.992	7.633	0.608	2.006	2.006
$\xi_{10}$	$X_{\text{bac}}$	0.306	0.268	0.346	0.059	0.059
$\xi_{11}$	$X_{\text{ac}}$	0.016	0.014	0.018	0.003	0.003
$\xi_{12}$	$X_{\text{ash}}$	14.84	35.344	28.344	19.142	19.142
$\xi_{13}$	$S_{\text{ion}}$	-0.02	-0.012	0.037	0.001	0.001
$\xi_{14}$	$S_{\text{ac-}}$	1.528	4.86	2.483	4.525	4.525
$\xi_{16}$	$S_{\text{nh3}}$	0.0	0.0	0.0	0.044	0.044

### A.3.2 Normalization Vectors

Table A.3: State normalization vector  $\underline{T}_x$

State	Normalization value
$S_{ac}$	0.137[g L <sup>-1</sup> ]
$S_{ch4}$	0.013[g L <sup>-1</sup> ]
$S_{IC}$	4.79[g L <sup>-1</sup> ]
$S_{IN}$	0.95[g L <sup>-1</sup> ]
$S_{h2o}$	958.0[g L <sup>-1</sup> ]
$X_{ch,f}$	2.59[g L <sup>-1</sup> ]
$X_{ch,s}$	8.09[g L <sup>-1</sup> ]
$X_{pr}$	1.46[g L <sup>-1</sup> ]
$X_{li}$	0.624[g L <sup>-1</sup> ]
$X_{bac}$	1.45[g L <sup>-1</sup> ]
$X_{ac}$	0.421[g L <sup>-1</sup> ]
$X_{ash}$	14.0[g L <sup>-1</sup> ]
$S_{ion}$	0.049[g L <sup>-1</sup> ]
$S_{ac-}$	0.137[g L <sup>-1</sup> ]
$S_{hco3-}$	4.42[g L <sup>-1</sup> ]
$S_{nh3}$	0.03[g L <sup>-1</sup> ]
$S_{ch4,gas}$	0.38[g L <sup>-1</sup> ]
$S_{co2,gas}$	0.569[g L <sup>-1</sup> ]
$V_{ch4}$	296.0[m <sup>3</sup> ]
$V_{co2}$	296.0[m <sup>3</sup> ]

Table A.4: Input normalization vector  $\underline{T}_u$

Corresponding substrate	Normalization value [m <sup>3</sup> /d]
Corn silage	80
Grass silage	80
Cattle manure	450
Sugar beet silage	80

### A.3.3 Substrate Costs

Table A.5: Costs of individual substrates

Substrate	Cost [€/t]
Cattle manure	20
Maize silage	40
Grass silage	35
Sugar beet silage	50

## A.4 Software - UML Diagrams

The entire information about an application scenario is specified within an instance of the 'Scenario' dataclass. Some of the required information for this instance includes normalization vectors, the selection of the optional gas storage model, the utilized substrates, disturbances, the number of days the simulation is supposed to run as well as the Model Predictive Controller. The latter is set up itself by instantiating the 'ControllerParams' class. Similarly, disturbances are instantiated through the 'Disturbances' class.

Since the sub-scenarios only differ through the introduced disturbances, a factory class was created for a less verbose instantiation of 'Scenario' instances. This only required the specification of the main scenario as well as the controller parameters. All other 'Scenario' parameters were set to presets but could be customized individually if necessary.

Substrates were represented by instances of the 'Substrate' class. Some of the parameters required for the instantiation were the cost of the substrate, the nominal  $\xi$ -values and variation coefficients for macronutrient related parameters as well as its state - liquid or solid.

The core class of the code developed for this thesis is the 'Simulation' class. Upon initialization it requires an instance of the previously described 'Scenario' class. It only features two public methods, 'setup' and 'run'. They in turn call private methods to either set up the entire simulation, i.e. configure and normalize the model, set up the Matplotlib and pygame based visualizations, set up the estimator, etc. or run the steady-state and the actual NMPC simulation. The code written for this thesis is available on GitHub: [https://github.com/JuliusFrontzek/ad\\_meal\\_prep\\_control](https://github.com/JuliusFrontzek/ad_meal_prep_control). The UML diagrams in Figures A.13, A.14 and A.15 visualize the software architecture of this work.

## Bibliography

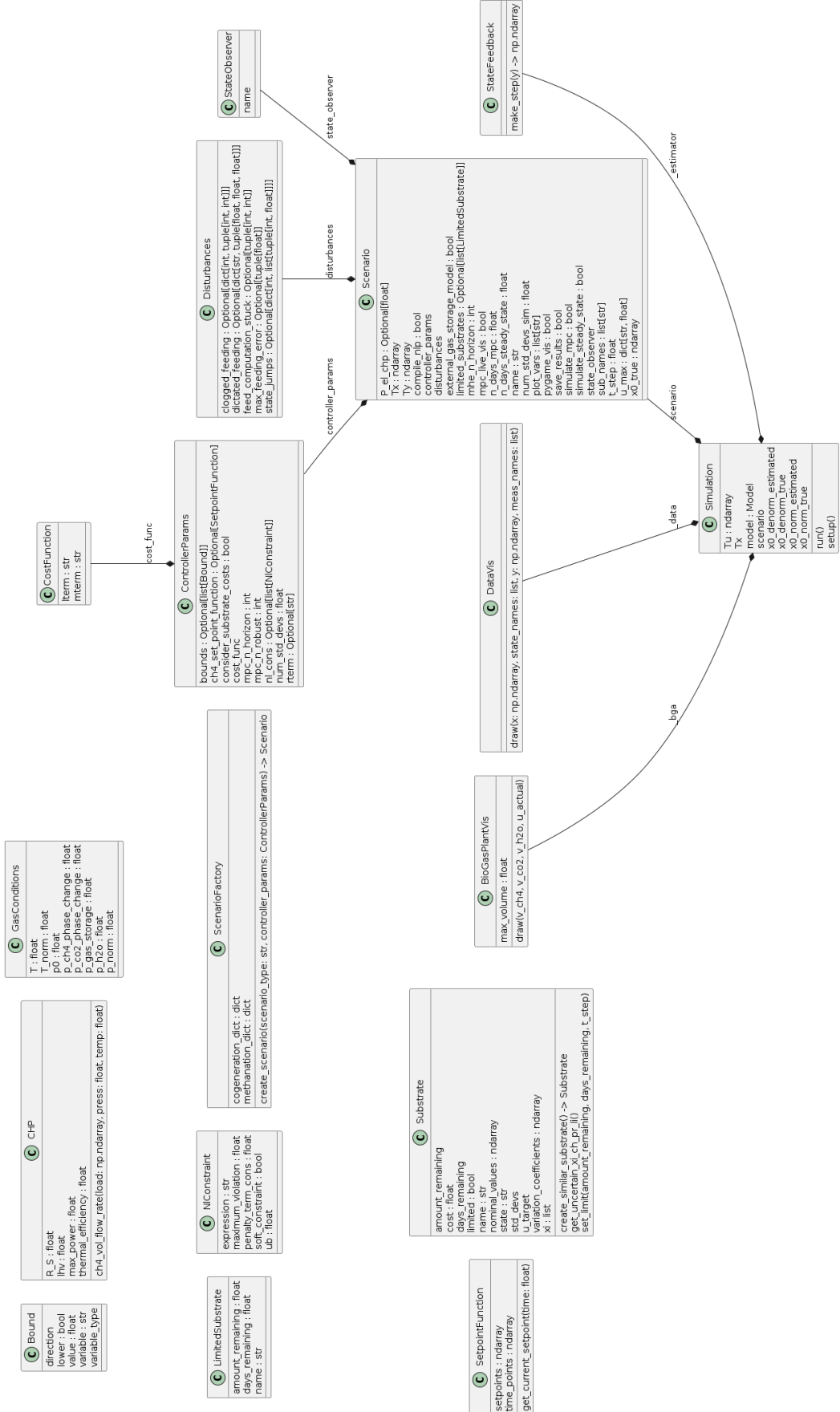


Figure A.13: UML class diagram for simulation code

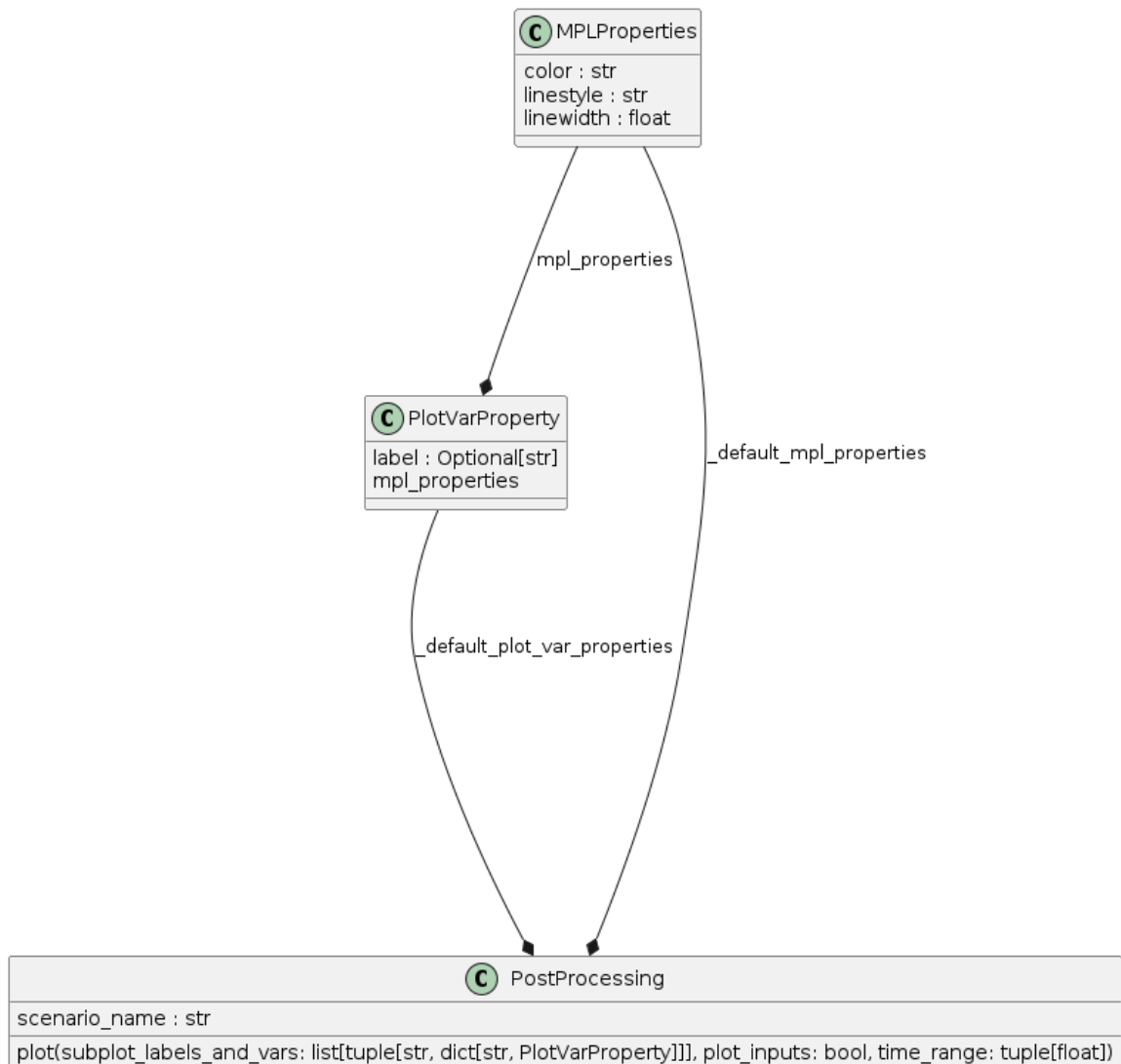


Figure A.14: UML class diagram for plotting code

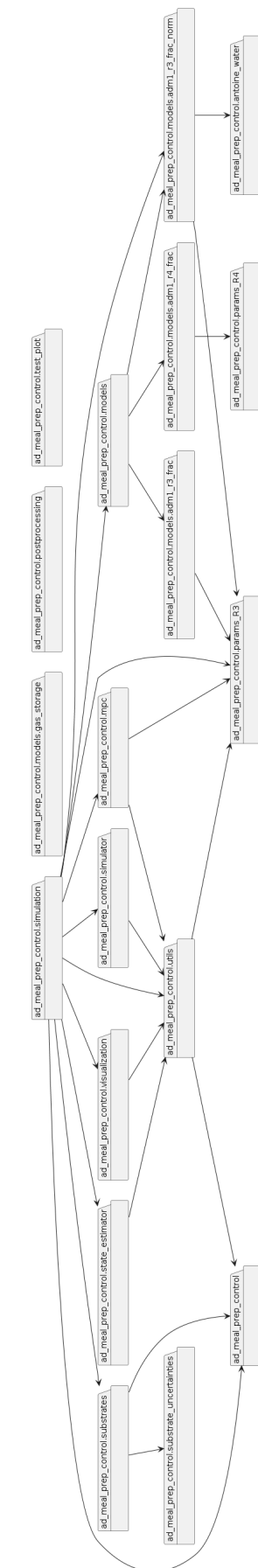


Figure A.15: UML package diagram



## A.5 DOC 2023



### INTRODUCTION

A mass-based simplification of the Anaerobic Digestion Model No. 1, called ADM1-R3, proposed by [1] allows for the embedding in a model predictive control (MPC) loop. The basic principle of MPC is illustrated in Fig. 1. The goal is to optimize the trajectory of substrates fed into the biogas plant such that a maximum amount of biogas is produced while avoiding process inhibition.

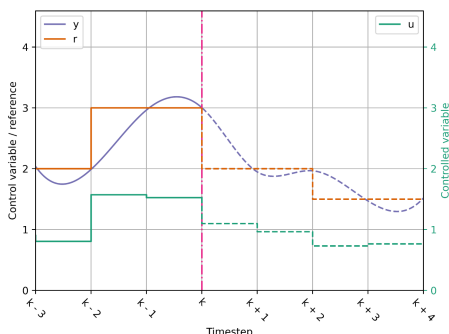


Fig. 1: Exemplary illustration of a model predictive control algorithm. Control variable ( $y$ ), reference ( $r$ ), and controlled variable ( $u$ ) depicted. Solid lines: Actual past values; dashed lines: Computed future values; dash-dotted line: Current time

### METHODS

The MPC algorithm was implemented using the Python-based open source library 'do-mpc' [2]. The system of ordinary differential equations was discretized by using orthogonal collocation on finite elements and solved using CVODES [3]. The ADM1-R3 was extended by a gas storage model which comprises a mixture of methane ( $\text{CH}_4$ ), carbon dioxide ( $\text{CO}_2$ ) and water vapor ( $\text{H}_2\text{O}$ ) as illustrated in Fig. 2. Disturbances such as random uniform errors for the feeding volumes were introduced.

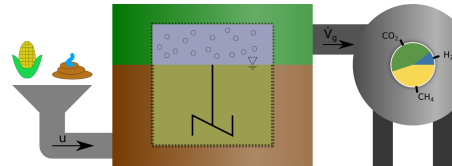


Fig. 2: Modeled biogas process extended by gas storage. Left: Agricultural substrate feed; center: fermenter with liquid (bottom) and gaseous phase (top); right: gas storage

### RESULTS AND OUTLOOK

Biogas outflow setpoint changes were successfully met within three hours while allowing for random uniform feeding errors of up to 5% as shown in Fig. 3.

As a next step, a multi-stage approach will be used to account for uncertainties in input feed concentrations. Further, different load cases will be examined.

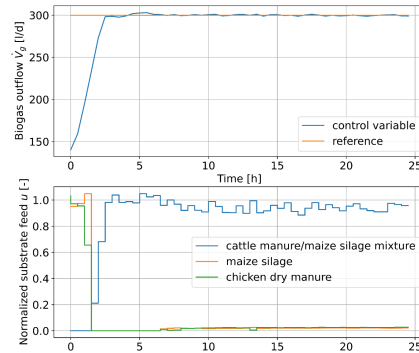


Fig. 3: Step response of Biogas outflow in the presence of a random uniform feeding volume error of +/- 5%

### REFERENCES

- [1] Weinrich, S., Nelles, M. (2021): Systematic simplification of the Anaerobic Digestion Model No. 1 (ADM1) - Model development and stoichiometric analysis. Bioresource technology, 125124.
- [2] Lucia, S., Tatulea-Codrean, A., Schopfmyer, C., and Engel, S. (2017): Rapid development of modular and sustainable nonlinear model predictive control solutions. Control Engineering Practice, 60:51-62
- [3] Gardner, D. and Reynolds, D. and Woodward, C. and Balos, C. (2022): Enabling New Flexibility in the SUNDIALS Suite of Nonlinear and Differential/Algebraic Equation Solvers. ACM Transactions on Mathematical Software (TOMS), 10.1145/3539801

**DBFZ Deutsches Biomasseforschungszentrum gemeinnützige GmbH** | Torgauer Straße 116 | 04347 Leipzig | www.dbfz.de  
Corresponding author: Julius Frontzek | E-Mail: julius.ferdinand.frontzek@dbfz.de | Telefon: +49 (0) 157 35549236

<sup>1</sup> Deutsches Biomasseforschungszentrum, Biochemical Conversion Department, Leipzig, Germany  
<sup>2</sup> Technical University of Berlin, Faculty of Process Sciences, Chair of Control, Berlin, Germany  
<sup>3</sup> Chemnitz University of Technology, Chair of Automatic Control and System Dynamics, Chemnitz, Germany  
<sup>4</sup> Münster University of Applied Science, Faculty of Energy, Building Services & Environmental Engineering, Münster, Germany



Figure A.16: Poster presented at the 6th Doctoral Colloquium BIOENERGY, Göttingen, on 18th/19th September 2023 displaying preliminary results of this work. The colloquium was organized by the University of Applied Sciences and Arts Hildesheim/Holzminden/Göttingen (HAWK).